Alma Mater Studiorum ï Università di Bologna

DOTTORATO DI RICERCA IN SCIENZE BIOMEDICHE

Ciclo XVIII

SC 06/F4, SSD MED/33

TUMOR MICROENVIRONMENT AS A TARGET OF OSTEOLYTIC BONE METASTASES

Presentata da

Dott.ssa Silvia Lemma

Coordinatore Dottorato

Chiar.mo Prof. Lucio I. Cocco

Tutor

Chiar.mo Prof. Nicola Baldini

Correlatore

Dott.ssa Sofia Avnet

Esame finale anno 2016

TABLE OF CONTENTS

ABSTRACT

Bone is one of the most common sites of distant metastases from breast carcinoma. In lytic bone metastasis, tumor associated-osteoclasts are the main actors of bone resorption. Under physiological conditions, osteoclast formation is activated by cytokines and hormones produced by bone-resident cells, including osteoblasts and mesenchymal stem cells. However, when tumor cells spread to the bone, they disrupt the delicate balance between cells orchestrating osteoclast formation, thereby promoting bone resorption. Current treatments of metastatic bone disease are largely ineffective to improve patient survival, possibly due to their inability to interfere with the metabolic pathways that regulate the behavior and the cross-talk between cancer cells and osteoclasts. To add news insights into the complex pathogenesis of osteolytic metastases, we focused our investigations on the role of lactate in the metabolic symbiosis of bone metastasis. We found that human osteoclasts are characterized by an increased mitochondrial metabolism, that probably supports the biosynthetic needs for osteoclast formation and activation, and that a glycolytic switch support the resorption activity of osteoclasts. Moreover, osteoclasts are able to uptake lactate from the extracellular space, an energy-rich metabolite produced by the glycolytic metabolism of breast carcinoma cells. In osteoclasts, lactate fuels oxidative metabolism, thereby increasing tumor aggressiveness. However, the bone metastatic microenvironment is composed of several types of cells, including tumor-associated stromal cells, bone-resident cells, tumor cells, and cancer-initiating cells. Each cell type takes part to the complex process of metastatic lesions formation. In particular, cancer stem cells play a primary role in tumorigenesis. To gain a more in-depth knowledge on the interplay between cells of tumor bulk, we validated the most stable housekeeping genes for gene

expression analysis on cancer stem cells. These findings lay the groundwork for future investigations on the cross-talk between stroma and tumor cells of the metastatic microenvironment.

Figure legend

Figure 5.1. Lactate exchange between highly glycolytic cells and osteoclasts in bone microenvironment supports tumor aggressiveness.

Table legend

Table 3.1. Candidate HKG genes.

Table 4.1. Transcriptome data from deep sequencing analysis of CSC and native osteosarcoma cells.

Table 4.2. Ct values of candidate HKG genes in CSC and native cell lines.

Table 4.3. Ranking of the stability of expression of candidate reference genes by NormFinder, geNorm, and CV analyses.

Table 4.4. Ranking of the stability of expression of candidate reference genes by NormFinder, geNorm, and CV analyses in CSC and native cells from carcinomas and sarcomas.

Abbreviations

18S rRNA: 18S ribosomal RNA

Ŭ-MEM: alpha-Modified Eagleôs Medium

ɸCt: delta cycle threshold

ACTB: actin, beta

ATP: adenosine triphosphate

B2M: beta-2-microglobulin

BMP: bone morphogenetic protein

CAF: cancer-associated fibroblast

CHC: alpha-cyano-4-hydroxy-cinnamate

CSC: cancer stem cell

COXII: cytochrome c oxidase subunit II, mitochondrial

CV: coefficient of variation

Ct: threshold cycles

DMEM: dulbecco's modified eagle medium

ECAR: extracellular acidification rate

FBS: fetal bovine serum

FCCP: carbonyl cyanide 4-trifluoromethoxy phenylhydrazone

FGF: fibroblast growth factor

G6PD: glucose-6-phosphate dehydrogenase

GAPDH: glyceraldehyde 3-phosphate dehydrogenase

GCT: giant-cell tumor of bone

GUSB: beta-glucuronidase

HKG: housekeeping gene

HMBS: hydroxymethylbilane synthase

HPRT1: hypoxanthine phosphoribosyltransferase 1

HSP60: heat shock protein 60 kDa

IGF-1: insulin-like growth factor-1

IGF-2: insulin-like growth factor-2

IMDM: Iscoveôs modified Dulbeccoôs medium

K_m: Michealis Menten constant

LDH: lactate dehydrogenase

M-CSF: macrophage colony-stimulating factor

MCT1: monocarboxylate transporter 1

MCT2: monocarboxylate transporter 2

MCT3: monocarboxylate transporter 3

MCT4: monocarboxylate transporter 4

MCT8: monocarboxylate transporter 8

MCT10: monocarboxylate transporter 10

MtOCR: mitochondrial OCR

NDUFB8: NADH dehydrogenase [ubiquinone] beta subcomplex subunit 8, mitochondrial

NFkB: nuclear factor-kappa B

OCR: oxygen consumption rate

OPG: osteoprotegerin

OPN: osteopontin

OXPHOS: oxidative phosphorylation

PBMC: peripheral blood mononuclear cells

PCR: polymerase chain reaction

PDGF: platelet-derived growth factor

PET: positron emission tomography

PGC-1ɓ: peroxisome proliferator-activated recepto-ɔ coactivator 1ɓ

PGK1: phosphoglycerate kinase 1

PPIA: peptidylprolyl isomerase A (cyclophilin A)

PTH: parathyroid hormone

PTHrP: parathyroid hormone-related peptide

qRT-PCR: quantitative real time polimerase chain reaction

RANKL: receptor activator of nuclear factor-kappa B ligand

RIN: RNA Integrity Number

ROI: region of interest

RPL13a: ribosomal protein L13a

SEM: standard error of mean

SD: standard deviation

SDHA: succinate dehydrogenase complex, subunit A, flavoprotein (Fp)

SDHB: Succinate dehydrogenase complex iron sulfur subunit B, mitochondrial

SLC: solute carrier

SDpooled : pooled standard deviation

TAT1: T-Type amino acid transporter 1

TBP: TATA-binding protein

TCA: tricarboxylic acid

TGF-ɓ: transforming growth factor beta

TRAP: tartrate-resistant acid phosphatase

TUBB: tubulin, beta class I

UQCRC2: Ubiquinol-cytochrome C reductase core protein II, mitochondrial

V-ATP5A: ATP synthase subunit alpha, mitochondrial

V-ATPases: vacuolar H(+)-ATPases

YWHAZ: tyrosine 3-monooxygenase/tryptophan 5-monooxygenase activation protein zeta polypeptide

1. INTRODUCTION

1.1 Metastatic bone disease

Cancer progression to metastasis is of dismal prognosis. Metastases derive from the dissemination and growth of neoplastic cells from the primary tumor to distant organs and tissues in the body. Bone is the most common site of metastases from solid tumors, and bone metastases are far more frequent than primary tumors of bone. Approximately 14 millions of new cancer cases are diagnosed each year worldwide [1], and up to 70% develop skeletal metastases [2].

Bone is a metabolically dynamic tissue that undergoes continuous remodeling throughout life. Bone homeostasis is maintained through a delicate balance between bone formation and resorption, mediated by bone-forming osteoblasts and bone-resorbing osteoclasts [3]. This coupling process is lost when cancer metastasizes to the bone [4]. An ample body of work has been performed to elucidate the key factors that are accountable for the loss of equilibrium between bone formation and bone resorption, which is responsible for the deleterious complications associated with bone metastases. Although in the early stages bone metastases can be asymptomatic, they are a devastating complication for most patients with advanced cancer. Lytic bone metastases are associated with a significant degree of morbidity related to osteolysis. The skeletal-related events result in intractable pain and other local complications, such as pathological fracture, spinal cord, and nerve root compression [5]. In the late phases of the disease, extensive bone destruction can lead to hypercalcemia, the most rapidly fatal complication of bone metastases [6]. All the skeletal-related events of

metastatic bone disease result in restricted mobility, greatly reducing the patientôs quality of life.

The management of patients with bone pain is multidisciplinary, including the use of analgesia, radio/chemotherapy, surgery, hormone therapy, opioids, and bisphosphonates (pamidronate and zeledronic acid). Analgesia, based on the use of non-steroidal anti-inflammatory drugs, is the first option in most patients, progressing to opioids as the intensity of pain increases. These agents produce several side effects, such as nausea, sedation, and constipation. Surgery can be used for localized metastatic disease, and hemibody radiation might be curative for patients with disease extending to one region of the body. In patients with widespread bone metastases, radiopharmaceuticals provide pain-control. However, current therapies are mainly palliative: to date, no effective treatment has been developed that is able to specifically target bone metastases.

1.1.1 **Normal bone physiology**

To understand the microenvironment of osteolytic metastases, an overview of the basic structure and function of bone is necessary.

Bone is the main structural and supportive connective tissue of the body. The majority of bone is formed by bone matrix, composed primarily of Type I collagen mineralized with hydroxyapatite crystals. Within these mineralized structure are trapped numerous growth factors, which are released upon bone resorption. The normal osseous tissue is composed by cortical and trabecular bone. The cortical or compact bone is the supporting part of the skeleton, made up of a dense layer of bone tissue. The trabecular or cancellous bone is the porous, metabolically dynamic part of bone matrix, typically located at the ends of long bones and within vertebrae. Under normal conditions, bone continually undergoes remodeling in a coupled and sequential process of osteoclast-

mediated bone resorption and osteoblast-mediated bone deposition. This remodeling cycle is tightly regulated to maintain bone structure and calcium homeostasis. To this purpose, many hormones and protein factors are involved in the cross-talk between osteoclasts, osteoblasts and other cells of bone microenvironment [7].

1.1.1.1 **Osteoblast biology**

Osteoblasts are mononuclear bone-forming cells with the specific function of regulating bone mineralization and synthesizing collagen precursors of bone matrix that form osteoid.

Osteoblasts derive from bone marrow mesenchymal stem cells (MSC). MSC proliferate and form pre-osteoblasts that differentiate into osteoblasts when stimulated by bone morphogenic proteins (BMP) and other growth factors. Afterwards, osteoblasts become osteocytes when trapped and surrounded by the bone matrix that they produce.

Osteoblasts take part in the control of osteoclast differentiation through the expression of the receptor activator of nuclear factor-kappa B (NFkB) ligand (RANKL), and the secretion of osteoprotegerin (OPG), a decoy RANKL receptor that blinds to RANK and inhibits osteoclast formation and activity. Osteblasts express on they surface different other molecules that are important for bone regulation, including parathyroid hormone (PTH) receptors, estrogen, vitamin D3, and different cytokines [8]. Several factors, such as PTH, prostaglandin E (PGE), fibroblast growth factor (FGF), transforming growth factor beta (TGF-ϐ), and RANKL have been shown to stimulate both resorption and formation of bone. Notably, PTH is the only known agent that is currently available for pharmacological stimulation of bone formation [9].

1.1.1.2 **Osteoclast biology**

Osteoclasts are giant, multinucleated, non-proliferative bone-resorbing polykaryons formed by the differentiation and fusion of hematopoietic stem cells (HSC) of the monocyte-macrophage lineage [10]. As shown in figure 1.1, these precursor cells differentiate into pre-osteoclasts, which fuse to form inactive osteoclasts. These are then activated, and became mature osteoclasts that are prone to resorb bone. The process is supported by two essential cytokines, the macrophage colony-stimulating factor (M-CSF) [11] and RANKL [12-14]. RANKL, in the presence of M-CSF, promotes the fusion of precursor cells to form multinucleated osteoclasts. In addition to RANKL, osteoblasts and several other cell types of bone microenvironment produce OPG, the decoy protein for RANK. The RANKL/OPG ratio is a central regulator of osteoclast differentiation at different steps, also involved in the activation of mature osteoclasts to resorption [15].

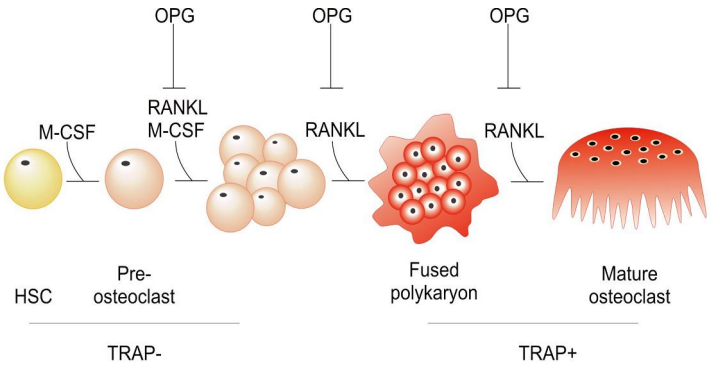

Figure 1.1. Osteoclast differentiation from hematopoietic precursor cells. Multiple molecules within the bone microenvironment drive osteoclastogenesis, including M-CSF, RANKL and OPG. RANKL and OPG levels regulate osteoclast differentiation at different steps.

It is accepted that osteoclast differentiation is orchestrated by these cytokines that are locally produced by osteoblasts, MSC and other cells of bone

microenvironment [16-18], as well as by growth factors [19], and systemic hormones [20]. Beside protein factors, osteoclastogenesis is also regulated by the modulation of physical conditions of bone microenvironment. In particular, reduced oxygen tension is a general stimulator of cells derived from marrow precursors [21]. Previous studies have elucidated that hypoxia is a potent stimulator of osteoclast differentiation when combined with periods of re-oxygenation [22], and increases osteoclast-mediated bone resorption [23], although it reduces the viability of mature osteoclasts [24,25]. Hypoxia is also associated with local acidosis, and reduced pH is an additional activator of mature osteoclast functions [26]. As a consequence, hypoxia and low pH are general features of various osteoclast-associated skeletal diseases [27,28].

More recent findings have elucidated that energy metabolism plays a central role in osteoclastogenesis and in the regulation of osteoclast activation to resorption [29]. Osteoclastogenesis is an energy-consuming process: the serial process of osteoclast differentiation from hematopoietic precursor cells requires high metabolic activity and ATP production [29,30] for proliferation of precursors, migration, and fusion to form multinuclear cells. Jin and colleagues have demonstrated that the presence of intact mitochondria is mandatory for osteoclastogenesis [31]. Mature osteoclasts are mitochondria-rich cells [32,33], which exhibit high expression of tricarboxylic acid (TCA) cycle and oxidative phosphorylation (OXPHOS) enzymes [34]. As confirmation, deletion of the co-trascriptional factor PGC-1ϐ in osteoclast precursors impairs osteoclast differentiation and mitochondrial biogenesis [35-37], outlining the importance of functional mitochondria in these cells [38].

1.1.1.3 **Mechanism of osteoclast-mediated bone resorption**

The specialized role of mature osteoclast is to polarize onto bone, bind to bone matrix via integrin proteins, and secrete acid and lysosomal enzymes in the extracellular resorption lacunae, which dissolve both inorganic and organic components of the bone matrix [39].

When osteoclasts are activated for resorption, they first reorganize the cytoskeleton to support its activity [40,41]. Podosomes mediate the attachment of osteoclasts to the extracellular matrix via the $\alpha_v\beta_3$ integrin [42], and contribute to form circular structures in the plasma membrane facing the bone matrix [43]. Podosomes disappear when F-actin forms the characteristic ring-like structures close to the bone facing plasma membrane. Ultrastructure of the sealing zone area reveals a tight attachment of osteoclasts to the bone surface via integrins, and this structure demarcates actual resorption areas [43].

After attachment of osteoclasts to the mineralized matrix, osteoclasts polarize the plasma membrane to form two specific membrane domains, the ruffled border and the functional secretory domain. The ruffled border membrane is the resorbing organ of osteoclasts. Osteoclasts activated to resorption secrete a large amount of acidic intracellular vesicles, which fuse with the plasma membrane facing to the bone surface inside the actin ring [44]. The process of osteoclast-mediated bone resorption demands the secretion of large amounts of protons and hydrochloric acid mediated by proton pumps, such as the vacuolar H(+)-ATPases (V-ATPases), to dissolve hydroxyapatite crystals, and the synthesis and secretion of proteases that degrades collagen fibers. During bone destruction, osteoclasts migrate along the bone surface, and support endocytosis and transcytosis of degradation products from the resorption lacunae [45-47]. In order to fulfill these functions, osteoclasts require high energy, considerable ion movement, and intense intracellular replacement of membrane material via vesicular trafficking. The activity of V-ATPases to pump protons in the

resorption lacunae is also an energy-consuming process, which requires high amounts of ATP [48].

1.1.2 The evolution of tumor metastasis

Metastasis is the final stage of tumor progression. Although the genetic basis of tumorigenesis can greatly vary, the steps of metastasis are similar in all tumors. Cancer evolution to metastasis is a multi-step process including multiple barriers to cancer cell dissemination. Cells from the primary tumor detach from adjacent cells, and invade the adjacent tissue in the primary organ (invasion). These cells then enter into tumor capillaries (intravasation), and via these capillaries reach the general circulation to colonize secondary sites (extravasation) [49]. Each of these steps represent cell interactions caused by specific characteristics of both tumor cells and the surrounding tissue [50].

Angiogenesis is the first and essential step for both the growth of the primary tumor and the metastatic process. Vascularization increases the supply of nutrients to tumors and the chance for tumor cells to migrate into tumor capillaries. The process of migration of cells into tumor capillaries (invasion) is stimulated by angiogenic factors produced by the tumor, and involve the adhesion of tumor cells to the basement membrane through adhesion molecules, and the secretion of matrix proteases and proteolytic enzymes to disrupt the basement membrane. Tumor cells in the circulation must overcome the stress imposed by hemodynamic shear forces and the assault by natural killer cells. Only a few, heavy-duty cells survive to circulation and arrive at the secondary site.

The process of migration of tumor cells into blood vessels at the primary tumor site are analogous to those involved in the migration from vasculature to the bone marrow cavity (extravasion). The extravasion process involves the

adhesion of tumor cells to other cells and matrix proteins of the secondary site, and the subsequent adaptation to foreign tissue microenvironment. In bone, tumor cells actively proliferate and adapt to grow [49,51].

1.1.3 Pathophysiology of bone metastasis

Metastases to bone frequently affect the axial skeleton, the anatomic site of red marrow in adults. Some authors have suggested that the distribution pattern of bone metastases could be in part justified by the pattern of distribution of regional venous drainage [52]. However, tumors also metastasize to distant organs that cannot be expected based on blood flow patterns. Most evidence suggests that not only the properties of circulation, but rather cells-to-cells and cell-to-extracellular matrix interactions within the axial skeleton could assist cancer cells in the formation of bone metastases [5,53,54]. The process is regulated by the activation of specific genes and by protein factors such as chemokines or motility factors. In summary, the formation of bone metastases is influenced by physical and cellular elements of the local region, suggesting that the specific site of spread of tumor cells is not only randomly determined by blood flow. This not-random concept for tumor metastases formation was proposed over a century ago by Stephen Paget [55], who referred to the phenomenon of tumor spread to specific sites in the body as the ñseed and soilò hypothesis. Indeed, although virtually any malignancy can metastasize to bone, breast and prostate cancers display a particular osteotropism [6,56], an exceptional affinity to metastasize and grow in bone, which accounts for about 65-80% of skeletal metastases [57]. The mechanism underlying cancer organotropism are various and involve distinctive characteristics of both carcinoma cells that enable the growth in bone [58], and the bone microenvironment that provides a fertile soil onto which to grow.

1.1.4 Types of bone metastases

The most common human adult carcinomas metastasize with avidity to bone. In particular, breast and prostate carcinoma are the two tumor types those most commonly metastasize to the skeleton. Breast cancer predominantly causes osteolytic metastases, characterized by increased bone loss, whereas prostate cancer classically causes osteoblastic (or osteosclerotic) lesions associated with abnormal new bone formation [59]. In lytic bone metastases, bone loss is associated with osteolysis caused mainly by osteoclast stimulation, or by a marginally osteolytic action of cancer cells on bone, and is related to reduced osteoblast functions that are uncoupled with bone resoprtion [59,60]. However, the situation is more complex, and both processes are typically present, ultimately tipping the balance to bone loss, gain or the mix of two lesions. In fact, although breast cancer commonly results in osteolytic lesions, about 25% of patients also exhibit osteoblastic lesions [54].

1.2 Microenvironment of osteolytic metastases

The complex process of tumor metastasis involves reciprocal interplay between cancer cells and host stroma, and is strongly influenced by microenvironmental factors.

The active cross-talk between the bone microenvironment and breast tumor cells promotes a vicious cycle that contributes to cell proliferation and bone destruction [61-63]. In this vicious cycle, tumor cells, once established in bone, secrete factors and cytokines that promote osteoclast-mediated bone resorption. In turn, osteoclast activity stimulates tumor cells proliferation by the release of numerous proteic factors embedded in the bone matrix that act on cancer cells, thereby promoting bone destruction and a more aggressive phenotype of tumor

cells [59,60]. The following paragraphs will discuss how metastatic cancer cells affect bone microenvironment to support their proliferation and the formation of lytic bone lesions.

1.2.1 **Cellular elements of bone metastatic microenvironment**

Bone microenvironment is a complex structural and biological system that holds hematopoietic and mesenchymal cells of multiple lineages, the bone marrow stroma, the bone matrix and a sinusoidal blood supply. Many of these elements enhance the proliferation of tumor cells and the formation of osteolytic lesions. First, physical factors within the bone microenvironment may promote tumor growth, including low oxygen tension, acidic pH, and elevated extracellular calcium and phosphate levels. Second, many growth factors stored in the bone matrix contribute to tumor cell proliferation, including TGF-ϐ and insulin-like growth factor-I (IGF-I) and II (IGF-II). Finally, and probably most importantly, transient cells and bone-resident cells, including osteoclasts, osteoblasts, and osteocytes, may directly sustain tumor growth [62]. Transient cells include erythrocytes, myeloid and immune T cells, platelets, bone marrow hematopoietic and endothelial cells, and other cells of the immune system, as well as bone marrow-derived mesenchymal stem cells. All of these cells may support tumor growth and metastases through different pathways [64,65], and some them are thought to take part in the formation of the pre-metastatic niche [65,66]. The role of bone resident cells in promoting tumor proliferation and osteoclast activation in osteolytic metastases will be discussed in the next sections. Moreover, an increasing body of evidence suggests that cancer stem cells (CSC), a small subset of stem-like elements within the tumor mass, sustain tumor progression from tumor initiation to the formation of local and distant metastases [67].

Figure 1.2 illustrates the complex microenvironment of lytic bone metastases. The metastatic microenvironment holds many cellular elements that contribute to the formation of osteolytic metastases. As mentioned above, tumor cells interact with stroma and bone resident cells, including osteoclasts, to support tumor cells proliferation, osteoclast differentiation and bone resorption, thereby promoting the formation of osteolytic lesions. CSC sustain metastasis as well, through several direct and indirect molecular and cellular mechanisms [68-70]. CSC are thought to reside in the metastatic niche [71] formed by tumor-associated stromal cells, differentiated tumor cells, and bone resident cells. Both stromal and tumor cells orchestrate the process of self-renewal of CSC and their differentiation in tumor cells. Stromal cells produce and secrete proteic factors inducing CSC self-renewal, while tumor cells secrete factors that negatively impact on CSC self-renewal, thereby promoting their differentiation in tumor cells.

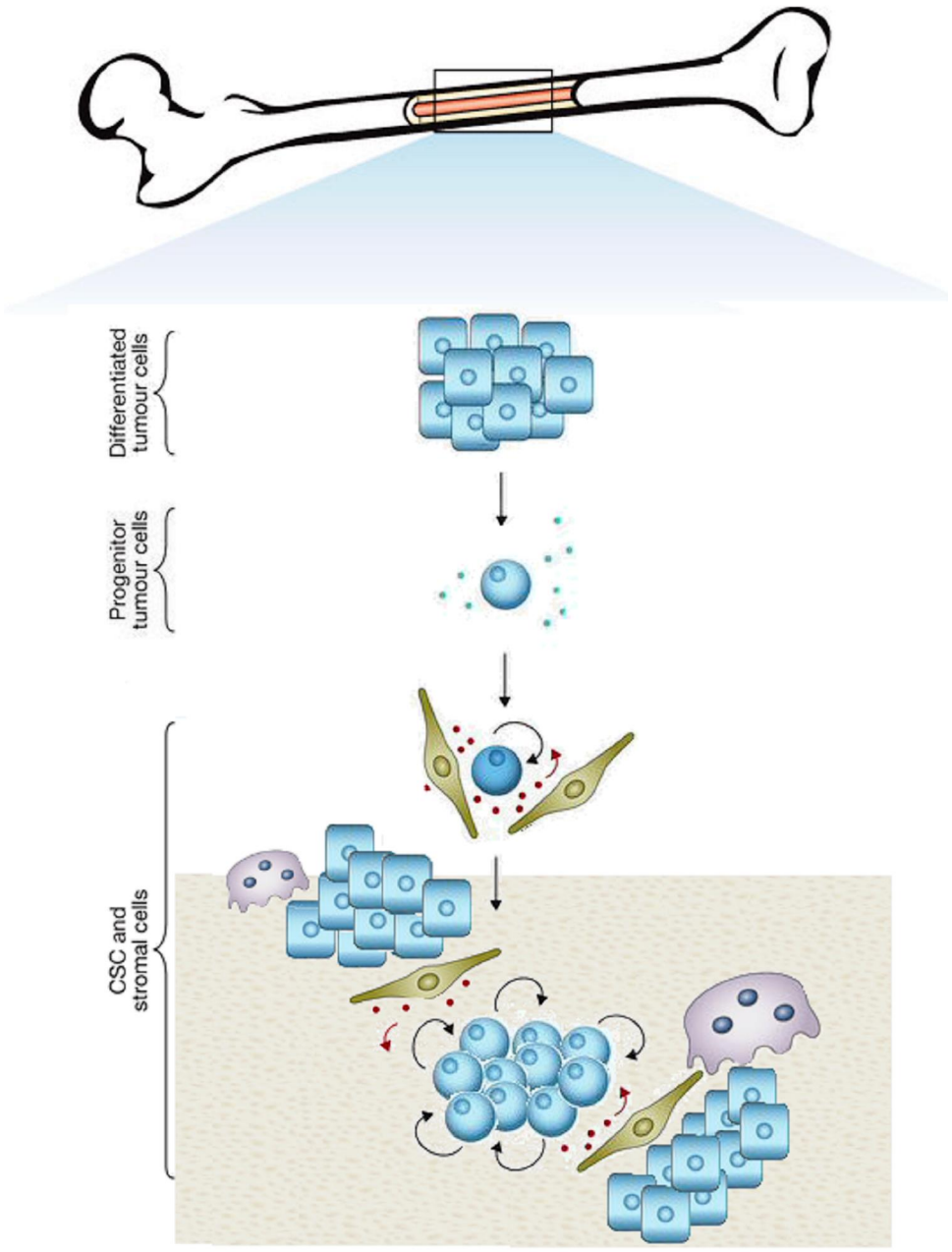

Figure 1.2. Cellular elements of bone metastatic microenvironment. In lytic bone metastasis, differentiated tumor cells, cancer stem cells (CSC), osteoclasts, and stromal cells interact to promote osteolytic lesions. CSC are a small subset of stem-like cells of the tumor mass. The proliferation of CSC is in part supported by proteic factors secreted by stromal cells.

1.2.1.1 Bone-resident cells sustain osteolytic metastases

In osteolytic metastases, the process of osteoclast differentiation and activation to resorption is supported not only by osteoblsts and MSC, but notably also by tumor cells that spread to bone. Breast cancer cells produce and secrete numerous osteotropic factors supporting osteoclastogenesis and osteoclast activity. The process of osteoclast stimulation can be mediated by cytokines released in the tumor microenvironment by tumor cells that induce osteoclast and their precurosor cells either directly or indirectly, through factors that stimulate osteoblast and MCS to release pro-osteoclastogenic cytokines [17,72,73]. One of the main activators of osteoclast activity is the parathyroid hormone-related peptide (PTHrP), which is expressed by up to 90% of metastatic human breast cancers [74]. Tumor-derived factors such as PTHrP bind to receptors expressed on osteoblasts and upregulate the expression of RANKL and M-CSF by cells of the osteoblastic lineage, i.e. osteoblast precursors, osteoblasts, and osteocytes. In turn, RANKL binds to its receptor RANK on osteoclast precursors to promote osteoclast recruitment and formation, as well as on mature osteoclasts to activate osteoclast-mediated bone resorption [75]. Osteoclast activity triggers the release of matrix-stored growth factors and cytokines, including TGF-ϐ, IGFs, platelet-derived growth factor (PDGF), bone morphogenetic proteins (BMP), which finally promote tumor cell survival and proliferation, and more extensive bone destruction by osteoclasts [4,76]. Thus, the development of lytic bone metastasis relies on an exquisite interplay between tumor and stromal cells, which promotes osteoclast-mediated bone destruction and increase tumor growth in bone.

1.2.1.2 Cancer stem cells

Stem cells are defined by their ability to self-renewal and to give rise to several differentiated cells for one specific organ. Similarly, CSC are a subpopulation of cells within the heterogeneous population of the tumor [77], which possess self-renewal and multilineage differentiation potential. It is thought that CSC are involved in various phases of tumor progression, from initiation to tumorigenesis [78], metastasis promotion [79-81], and resistance to chemo- or radiotherapy [82-84].

Advocates of the CSC model (also known as the hierarchy model) depict that tumors are hierarchically organized and maintained by CSC [85]. This small but distinct population of quiescent uncommitted cells can be isolated from the tumor mass for their ability to grow and proliferate in anchorage-independent conditions forming floating colonies, the so-called ñspheresò (Figure 1.3) [86,87]. CSC have been successfully isolated from hematological malignancies [88,89], and from different types of solid tumors [90,91], including sarcomas [92-94], from both immortalized cell lines [93,95] and tissue specimens [92,96,97].

Recent findings have elucidated that CSC differ from the respective native cells not only for the peculiar ability to grow as floating colonies, but also for morphological and stemness features, and for lysosomal acidity [92,93], which probably affect the energy metabolism.

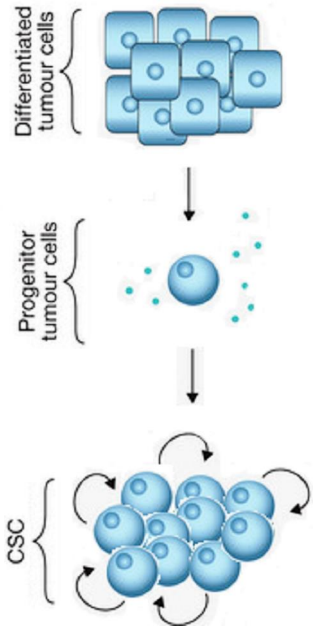

Figure 1.3 CSC model. CSC can be isolated from differentiated tumor cells by using the sphere-forming assay. A progenitor tumor cells is able to growth in conditions of anchorage-independence to form CSC with characteristics of stemness, self-renewal, tumor-propagating capacity in vivo, and metastasis formation.

The classical model of clonal selection of metastasis asserts that genetic mutation attained in the late steps of the tumorigenic process provide a selective advantage for metastasis formation. Nevertheless, recent findings have elucidated that the metastatic process is also supported by genetic mutations acquired in the initial stages of tumor development [98]. Accordingly, a genomic approach can highlight the molecular signature that predicts poor prognosis in cancer patients. In particular, recent functional genomic analyses have highlighted the cellular and molecular mechanisms that mediate the formation of tissue-specific metastases [99-101], providing evidence of the presence of a small subset of cancer cells within the heterogeneous mass of breast tumor cells that is already programmed to preferentially metastasize to specific organs [102]. Hence, tumor therapy should be directed at eliminating these tumor-initiating cells that are primarily responsible for resistance to conventional

approaches.

1.3 **Metabolic reprogramming in the tumor microenvironment**

Metabolism of cancer cells is different from that of normal cells. Cancer cells demands increased energy in form of ATP to support abnormal proliferation and macromolecular biosynthesis. In addition, the survival of migrating tumor cells outside the primary tumor niche requires adaptation of metabolism to several microenvironmental conditions.

Tumors are highly heterogeneous in all phenotypic features, including metabolism. The metabolic profile of tumor cells is controlled by multiple molecular mechanisms, including intrinsic genetic mutations and external response to tumor microenvironment [103]. Many oncogenic and tumor suppressor signaling pathways driving tumorigenesis are key regulators of metabolic networks [104], suggesting a tight link between metabolic alterations and tumor progression.

Most tumors and wounds are subjected to low oxygen tension [105], especially in the bone microenvironment [106,107]. Hypoxia selects cells to undergo the ñglycolytic switchò, a fundamental metabolic adaptation by which glycolysis is uncoupled from mitochondrial respiration and becomes the main supplier of cellular ATP [108]. Although tumor hypoxia can be transient, pioneer studies have highlighted that some tumor cells rely on glycolysis even in the presence of normal oxygen levels [109]. This is an apparent paradox, considering that glycolysis is far less efficient than OXPHOS in producing energy. In fact, the catabolism of glucose provide only 2 ATP molecules for each glucose that enters in the glycolytic pathway, whereas mitochondrial respiration provides 38 ATP molecules. Persistence of aerobic glycolysis is a feature of cancer cells and a

hallmark of advanced cancer, and involves stable genetic and epigenetic alterations of several oncogenes and tumor-suppressor genes that are still under investigation [108]. This phenomenon was first described by Otto Heinrich Warburg [110], and is referred as Warburg effect. Aerobic glycolysis is characterized by an increased glucose uptake and a large production of extracellular lactate and H+ in the tumor microenvironment, which causes a decrease of extracellular pH to levels lower that in normal cells [111]. The Warburg effect has significant medical application, as high aerobic glycolysis has been clinically proven in many malignant tumors. Strong evidence has indicated that the glycolytic phenotype confers significant growth advantage to cancer cells [112]. In clinical practice, glucose uptake by tumor cells is commonly visualized with positron emission tomography (PET) using a radiolabelled analogue of glucose (^{18}F-fluorodeoxyglucose).

Recent studies have shown that the Warburg effect is also activated in stromal cells of tumor microenvironment. In particular, cancer-associated fibroblasts (CAF) [113,114], that originate from MSC [115], produce energy-rich metabolites that can fuel tumor cell metabolism. Cancer cells are able to uptake energy-rich metabolites, such as ketones and lactate [116], and use them in the TCA cycle and in the mitochondrial metabolism. This phenomenon is known as the reverse Warburg effect [117]. This role of tumor-associated stromal cells as tumor feeders has been reported in different types of cancer, including human breast [116,118] and prostate carcinoma [119], osteosarcoma [120], and head and neck cancer [121].

1.3.1 Lactate as metabolic fuel in cancer: the metabolic symbiosis of tumor microenvironment

Tumor cells uptake more glucose that normal cells, and mainly process it through aerobic or anaerobic glycolysis. The increased glycolytic flux is associated with a high lactate production rate in malignant cells. In fact, the oxidation of glucose through glycolysis produces high levels of pyruvate, NADH and protons. Pyruvate, in turn, can be converted to lactate, the end product of glycolysis, in malignant, rapidly growing cells. Lactate production and excretion by malignant cells in solid tumors leads to a substantial accumulation of this metabolite in the tumor microenvironment [122]. Lactate, once considered a waste product of glycolysis, has recently emerged as a critical regulator of cancer development and a prominent metabolite that fuels the oxidative metabolism of oxygenated cells [123,124]. Lactate accumulation in human tumors is a predictor of poor prognosis, associated with metastasis, tumor recurrence, and patient survival [125-127].

Lactate metabolism is regulated by several factors, including lactate dehydrogenase (LDH) activity, the expression of monocarboxylate transporters (MCT) and the oxidative capacity of tissues. The use of lactate as an energy source requires, aside to its conversion to pyruvate and back, the transport of lactate across the plasma membrane through MCT. MCT proteins mediate the exchange of lactate between cells of tumor microenvironment, with MCT4 that facilitates lactate export, and MCT1 that promotes lactate uptake [128] (see below). Lactate exchange in the tumor microenvironment could fuel the oxidative metabolism of tumor cells [123], thereby creating a metabolic symbiosis between glycolytic and oxidative cells. In fact, as a result of the reverse Warburg effect, mesenchymal cells and CAF of tumor microenvironment secrete high levels of lactate, which can be uptaken by oxidative tumor cells to support their grow [123]. Once entered into the cytoplasm, lactate fuels the TCA cycle and mitochondrial respiration, providing

energy for the proliferation of oxidative cells. However, in the cancer microenvironment, lactate can be uptaken not only by oxidative tumor cells, but also by tumor supporting stroma, like vascular endothelial cells. Recent studies have elucidated that in endothelial cells lactate acts both as a signaling molecule and as a metabolic intermediate that stimulates endothelial cell migration, tube formation, and tumor angiogenesis [128-130]. Lactate can therefore act as an energy-transfer molecule in the tumor microenvironment, thereby fueling several energy-consuming processes in both tumor and tumor-associated stromal cells.

1.3.2 **Monocarboxylate transporters as lactate shuttles in cancer**

The transport of monocarboxylates, such as lactate, pyruvate and ketone bodies (acetoacetate and D-b-hydroxybutyrate) across the plasma membrane is crucial for several metabolic pathways, and is mediated by MCT [131,132]. Between these substrates, L-lactate is quantitatively by far the most important substrate in cancer metabolism. At physiological pH, lactate is more than 99% dissociated into protons and lactate anions. Since it is lactic acid rather than lactate that is produced and used in cell metabolism, the capacity of MCT to transport a proton with lactate is convenient for its metabolic roles.

MCT are encoded by the solute carrier (SLC)16 family, which is composed by 14 members. MCT1 (SLC16A1), MCT4 (SLC16A3), MCT2 (SLC16A7) and MCT3 (SLC16A8) facilitate the proton-linked transport of monocarboxylates in and out of cells. MCT10 (SLC16A10), also known as T-Type amino acid transported 1 (TAT1) is an aromatic amino acid transporter, and MCT8 (SLC16A2) is a thyroid hormone transporter [133].

The MCT are membrane proteins spanning the entirety of plasma membrane.

They are predicted to have 12 transmembrane domains, with the N- and C-terminal domains facing the cytosolic side of the membrane and a large intracellular loop between the domains 6 and 7. The MCT proteins present significant sequence identity in the 12 transmembrane domains, but differ mostly in the N- and C-terminal and in the loop sequences [133]. MCT proteins require ancillary proteins to be stably expressed at the plasma membrane. The ancillary proteins are single-membrane pass glycoproteins with extracellular immunoglobulin domains. MCT1, MCT3 and MCT4 associate with the chaperone basigin, also known as CD147, EMMPRIN or OX-47, whereas MCT2 preferentially associated with the chaperone embigin, also known as gp70 [134-136].

MCT facilitate both influx and efflux of monocarboxylates. The direction of net transport is determined by the concentration gradients of protons and monocarboxylate across the plasma membrane, and by the affinity for monocarboxylates between MCT proteins. The affinity for lactate and other monocarboxylates such as pyruvate between MCT is reflected by the Michealis Menten constant (K_m) value. MCT1 and MCT2 present low K_m (high affinity) for lactate (3-6 mM for MCT1, 0.5-1 mM for MCT2), suggesting their predominant role in the regulation of lactate uptake, whereas the low-affinity (high Km) of MCT4 for lactate (25-30 mM) indicates its role in the export of intracellular produced lactate.

The MCT proteins present different patterns of expression in organs and tissues. MCT1 is the most widely expressed MCT. It is involved in lactate uptake in the cardiac tissue, liver, skeletal muscle and red blood cells. MCT2 and MCT3 have a more restricted expression pattern. MCT2 is primarily expressed in liver, kidney and neurons in the brain, and in particular it plays key roles in neurons at the postsynaptic complex. MCT3 is expressed at the basolateral retinal pigment

epithelium and choroid plexus epithelia [137]. MCT4 expression is primary limited in highly glycolytic cells, such as white muscle fibers, and is upregulated in hypoxic conditions [138].

MCT1 and MCT4 are the most important lactate shuttles in tumor cells and represent promising targets for therapy. As mentioned above, several authors have elucidated that lactate exchange in tumors acts as a prominent fuel for the oxidative cells of tumor microenvironment, and MCT as crucial component of the metabolic symbiosis. In the tumor microenvironment, both oxidative tumor cells and endothelial cells close to tumor blood vessels can uptake lactate released by glycolytic cells [123,129], and used as main source of metabolic fuel by oxidative cancer cells [123]. Glycolysis-derived lactate is released in the extracellular microenvironment through the low-affinity lactate shuttle MCT4, whereas the exogenous lactate is uptaken by oxidative tumor cells through the high-affinity lactate shuttle MCT1. Lisanti and colleagues have provided evidence that cancer-associated fibroblasts can undergo aerobic glycolysis to support proliferation and metastasis of oxidative cancer cells with the released lactate and ketones [116,139]. Another study has reported that lactate can also enter tumor-associated endothelial cells through MCT1 [129], demonstrating that lactate not only supports the survival of serum-starved endothelial cells, but, more interestingly, dictate the pro-angiogenic signaling pathways that drive endothelial cell migration and tube formation. More recently, we have reported that reactive MSC in osteosarcoma increases lactate production as a result of the oxidative stress induced by adjacent tumor cells. Reactive MSC express high levels of MCT4 and release energy-rich metabolites that fuel the mitochondrial metabolism and the migratory ability of MCT-1 expressing osteosarcoma cells [120].

This evidence supports that altered microenvironmental conditions promote

metabolic reprogramming of cancer cells and their stroma, thereby suggesting that the impairment of metabolic symbiosis of tumor microenvironment is a target for cancer therapy.

1.4 **Bone tumor microenvironment as a target of cancer therapy**

Current knowledge suggests that the strict interplay between tumor and stromal cells in the bone microenvironment promotes tumor progression and metastasis, not only through the paracrine secretion of cytokines and proteic factors, but also via intermediate metabolites, which contribute to the metabolic reprogramming of tumor microenvironment. Such metabolic reprogramming is a common feature of both tumor and stromal cells, which function symbiotically. Stroma and bone resident cells are induced by cytokines produced by tumor cells, and, in turn, stromal and bone resident cells promote tumor progression and metastasis through the release of bone matrix-stored growth factors and chemokines. Moreover, stromal cells directly fuel tumor cells by exporting lactate and energy-rich metabolites through MCT shuttles, which are metabolized by adjacent tumor cells. As a consequence, alteration of the metabolic symbiosis can dramatically impair tumor growth.

Genetic knockdown studies and the synthesis of several small-molecule inhibitors of MCT shuttles have confirmed the potential relevance of targeting lactate transporters in cancer therapeutics. Sonveaux and colleagues have demonstrated that the inhibition of MCT1 through the small molecule alpha-cyano-4-hydroxy-cinnamate (CHC) [123] can shift the metabolism of the lactate-consuming oxidative cancer cells towards the glucose metabolism, thereby reducing the amount of glucose available for hypoxic tumor cells and impairing their survival. On the other hand, inhibition of MCT4 can potentially

target hypoxic cancer cells and promote their death by intracellular lactic acid accumulation. Other authors have shown that in tumor-associated endothelial cells, knockdown of the MCT1 and MCT4 shuttles determines a dramatic inhibition of angiogenesis mediated by endothelial cells, by reducing lactate uptake and extracellular lactate availability, respectively [129]. More convincingly, the inhibition of MCT1 with AR-C155858, a highly selective and potent MCT1/MCT2 inhibitor, blocks the proliferation and tumorigenicity of tumor-activated fibroblasts [140]. Furthermore, a second-generation MCT1/MCT2 inhibitor, AZD3965, is in Phase I clinical trials for patients with advanced solid tumors, prostate cancer, gastric cancer and diffuse large B cell lymphoma (Cancer Research UK. A Phase I Trial of AZD3965 in Patients With Advanced Cancer. https://clinicaltrials.gov/ct2/show/NCT01791595).

The exquisite metabolic symbiosis of the tumor microenvironment supports the development of MCT inhibition strategies. There is a real hope that agents that target lactate metabolism and transport between cells of the tumor microenvironment will substantially contribute to anti-cancer therapy. However, nothing is currently known about the role of lactate metabolism in lytic bone metastasis. To extend such strategies to efficient anti-bone metastasis therapy, a better understanding of lactate shuttling in osteolytic metastases is clearly needed.

2. AIM OF THE STUDY

The aim of this study was to evaluate the influence of the metabolic symbiosis between tumor cells and cells of bone microenvironment in lytic bone metastases. Osteolytic metastases are a devastating event for many patients with advanced breast cancer, often leading to a significantly decreased quality of life. Despite progress in understanding the molecular biology of metastatic breast tumor cells, to date there are no specific therapies for metastatic bone disease. Current treatments are mainly palliative. Hence, it is pivotal to gain a more in-depth knowledge on the metabolic regulation of lytic bone metastases, and the interplay between the cellular elements of the metastatic microenvironment. Consequently, during my doctoral training I focused on the previously mentioned issues.

In lytic bone metastases from breast cancer, tumor cells harness the osteolytic activity of osteoclasts to promote bone resorption and remodeling, thereby creating a metastatic niche. Osteoclasts and tumor cells support each other through a vicious cycle in which tumor cells produce cytokines that support osteoclast formation and activation, and osteoclast activity promotes the release of bone-embedded growth factors, which, in turn, promote tumor cell proliferation. However, we postulated that this mechanism is not exhaustive to explain the complex microenvironment of bone metastases, because high-energy metabolites produced by the peculiar metabolism of tumor cells can be even more relevant in this context. We supposed that in the tumor microenvironment, lactate produced by the glycolytic metabolism of breast tumor cells could be uptaken by osteoclasts to promote its oxidative metabolism, and support the energy-consuming process of bone destruction, thereby promoting osteolytic diseases. To verify this hypothesis of the metabolic symbiosis of tumor

microenvironment, during my doctoral training I first investigated the basal metabolism of human osteoclasts during osteoclastogenesis, then analyzed the metabolic adaptations underling the activation of mature osteoclasts to resorption, and subsequently analyzed the role of lactate in the interplay between tumor and bone-resident cells.

The microenvironment of osteolytic metastasis is heterogeneous, and involves many different actors, among which the most important are osteotropic tumor cells, cancer stem cells (CSC) and bone-resident cells. The contribution of CSC to metastatic diseases is currently an important focus of investigation. With the aim to lay the groundwork for analyses on the gene expression profile of CSC and native cells, during my doctoral training I also focused on the identification and validation of housekeeping genes for gene expression analysis of CSC and native tumor cells from breast and renal carcinoma, two osteotropic tumors, and sarcomas, primary tumors of bone.

3. MATERIALS AND METHODS

3.1 Cell culture

3.1.1 Human osteoclast cultures

Primary cultures of osteoclasts were obtained from monocytic precursors isolated from fresh buffy coats obtained from n.=15 different healthy donors (AVIS, Bologna, Italy; Saint-Luc University Hospital, Brussels, Belgium), as previously described [19]. Briefly, peripheral blood mononuclear cells (PBMC) were layered over Hystopaque (GE Healthcare) and seeded on tissue-culture glass or plasticware (3,000,000 cells/cm^2) in Dulbecco's Modified Eagle Medium (DMEM; Sigma) supplemented with 25 mM glucose (Merck), 10% heat-inactivated fetal bovine serum (FBS; Celbio), plus 20 U/mL penicillin, 100 mg/mL streptomycin (Euroclone), and incubated at 37 °C in a humidified 5% CO_2 atmosphere. All experiments were performed in pyruvate- and glutamine-free media buffered at pH 7.4 (3.7 g/liter NaHCO3) (complete DMEM), unless stated otherwise. After 2 hours, medium was discarded and replaced with complete DMEM added with RANKL [50 ng/mL] and M-CSF [10 ng/mL] (Peprotech) (pro-osteoclastogenic medium), or with complete DMEM without pro-osteoclastogenic factors (control medium), depending on the experimental conditions. In order to verify osteoclast differentiation, after 5 to 7 days of cell culture, cells were analyzed for tartrate-resistant acid phosphatase (TRAP) activity by cytochemistry (Acid Phosphatase Leukocyte assay, Sigma) and stained with Hoechst 33258. Only TRAP+ cells with 3 or more nuclei were considered as osteoclasts.

3.1.2 Growth condition and propagation of adherent tumor cell lines

Rhabdomyosarcoma cell line (RD), osteosarcoma cell lines (MG-63, HOS,

Saos-2), Ewingôs sarcoma cell line (A-673), breast carcinoma cell line (MDA-MB-231), renal carcinoma cell line (ACHN), and bone marrow derived MSC were purchased from American Type Culture Collection (ATCC). MDA-MB-231 bone metastasis cell line was kindly provided by Nadia Rucci (University of LôAquila, Italy) [141]. MSC were maintained in alpha-Modified Eagleôs Medium (Ŭ-MEM, Sigma), supplemented with 10% heat-inactivated FBS (Sigma), plus 20 U/mL penicillin (Gibco), 100 mg/mL streptomycin (Gibco). All the other cell lines were maintained in Iscoveôs modified Dulbeccoôs medium (IMDM, Gibco), plus 20 U/mL penicillin, 100 mg/mL streptomycin, and 10% heat-inactivated FBS (complete IMDM). All the cell lines were grown under controlled atmosphere in the presence of 5% CO_2 at 37 °C. Complete medium were prepared by filtering the mixture using a 0.2 ε m filter. Cells were grown in plastic cell culture flasks until 90% confluence. The medium was removed and washed once with PBS buffer, and 10% trypsin solution was added for 5 minutes. Fresh medium was added to block the protease action, cells were collected into a plastic tube and centrifuged for 5 min at 1000 rpm. The pellet was resuspended in fresh medium and placed in a new plastic flask.

A human primary ES culture (ES4540) was also used, previously obtained from a fresh biopsy of human ES, and characterized as previously described [92]. The ES4540 sample was collected after a signed informed consent and following the approval of the institutional ethical committee (0033626, 9 Nov 2011), according to the Declaration of Helsinki. Briefly, tissue samples were subjected to mechanical mincing, followed by enzymatic digestion, to obtain single cells that were seeded in complete IMDM until the formation of a monolayer.

3.1.3 Cancer stem cells cultures

CSC cells were obtained as previously described [92]. Briefly, RD, MG-63, HOS, Saos-2, A-673, MDA-MB-231, ACHN, and ES4540 cultures were

maintained in anchorage-independent conditions in DMEM:F12 medium with progesteron (20 nM), putrescin (10 mg/mL), sodium selenite (30 nM), apo-transferrin (100 ε g/mL), and insulin (25 ε g/mL) (Sigma-Aldrich, St. Louis, MO) in low-attachment flasks (Nunc, Penfield, NY) (sphere-forming assay). We obtained the CSC culture by maintaining the spheroid in anchorage-independent conditions in specific cell media, adding the growth factors EGF and bFGF every 3-4 days (twice at week). Fresh human EGF (20 ng/mL) and bFGF (10 ng/mL) (PeproTech, Rocky Hill, NJ) were added twice a week until cells started to grow as floating aggregates (spheres). Spheroid cultures were amplified by treating the primary CSC culture with trypsin, followed by gentle mechanical dissociation, and by re-plating single-cell suspension to obtain the second spheroid culture. Viability was verified by erythrosine staining. The percentage of dead cells was low (10-15% of dead cells). Only those cultures that were able to form spheres and that expressed stem cell-related markers were considered.

3.2 Metabolic assays

3.2.1 Glucose consumption and lactate production

Glucose consumption and lactate production were measured by analysing the metabolite content of deproteinized cell culture supernatants. PBMC were seeded as described above on 96-well plates in control media or pro-osteoclastogenic media and cultured until multinucleated TRAP+ cells were formed (around 7 days). To analyze osteoclast basal metabolism, media was then changed with fresh control media or pro-osteoclastogenic, respectively, and after additional 5 days, the supernatant was collected. To analyze the effect of lactate on osteoclast metabolism, media were then changed with fresh complete medium containg 10 mM sodium lactate (Sigma), or control media, and after additional 7 days the supernatant was collected. Metabolite concentrations were

quantified using specific enzymatic assays on CMA600 analyzer (CMA Microdialysis AB). Glucose consumption and lactate production were normalized on total protein content using the Bradford protein assay (Bio-Rad). Results were representative of 3 independent experiments, with 5 technical replicates for each condition.

3.2.2 Oxygen consumption and extracellular acidification measurement

Oxygen consumption rate (OCR) and extracellular acidification rate (ECAR) were determined using a Seahorse XF96 extracellular Flux analyzer with a mitostress kit (Seahorse Biosciences). To analyze osteoclast basal metabolism, PBMC were seeded on XF96 cell culture plate in control media or pro-osteoclastogenic media, and incubated from 2 to 14 days. To analyze the effect of lactate on osteoclast metabolism, after osteoclast formation (7 days) media was then changed with fresh complete medium containg 10 mM sodium lactate, or control media, and after additional 7 days cells were analyzed. Culture media were changed with base media (unbuffered DMEM supplemented with 25 mM glucose) 1 hour before. Selective inhibitors were injected during the measurements to achieve final concentrations of oligomycin [2 εM], Carbonyl cyanide 4-trifluoromethoxy phenylhydrazone FCCP [0.9 εM], rotenone [1εM] antimycin A [1εM], and 2-deoxy-glucose [100 mM]. Mitochondrial OCR (mtOCR) was assayed by injecting rotenone and antimycin to acutely inhibit mitochondrial-driven oxygen consumption. mtOCR was calculated by subtracting non-mitochondrial OCR from total OCR levels. ATP coupling were calculated by subtracting total OCR from oligomycin readings, which uncouples ATP synthesis from oxygen consumption. Data were normalized for total protein content using the Bradford protein assay. Results are representative of 3 independent experiments with 7 technical replicates each.

3.2.3 ATP assay

PBMC were seeded on 12-well plates and maintained in pro-osteoclastogenic media or control media until multinucleated TRAP+ cells were obtained (around 7 days). Two hours before the assay, media were changed with fresh pro-osteoclastogenic media or control media. Cells were washed and lysed by using boiling ATP lysis buffer [0.1 M Tris(hydroxymethyl) aminomethane (Tris base) (Sigma) and 2 mM EDTA adjusted to pH 7.75 with acetic acid (Sigma)]. Cell lysates were added to a reaction mixture containing luciferase and luciferine (ATP Determination Kit, Molecular Probes) for bioluminescence quantification by using Infinite® 200 PRO plate reader (Tecan). ATP level was normalized with total protein content (Bradford protein assay). Results were representative of 3 independent experiments, with 4 technical replicates each.

3.2.4 ^{14}C-Lactate uptake assay

PBMC were seeded on flat-bottom 24-well plates, and maintained in pro-osteoclastogenic media until osteoclast differentiation was obtained. When multinucleated TRAP+ cells were formed (around 7 days), the culture medium was replaced by pro-osteoclastogenic media containing 10 mM sodium lactate, and incubated overnight for metabolic adaptation. Cells were first rinsed with a modified Krebs solution (containing 10 mM L-lactate, without glucose), and exposed to increasing concentrations of 14C-L-Lactate (1, 2, 4, 8, 16 εM) or control Krebs solution at 37°C for 12 minutes. Cells were then rinsed with ice-cold D-lactate-containing Krebs solution (10 mM D-lactate, without glucose) and lysate with 0.1 M NaOH. Sample aliquots were then incubated in liquid scintillation solution (Microscint 40) into a 96-well plate (Optiplate). After a 1 hour agitation, radioactivity was measured (PerkinElmer Topcount). Cpm values

were nomalized per protein amount (Bradford protein assay).

3.3 Resorption assay

Resorption activity was measured by using the OsteoLyse bone resorption assay kit (Lonza). Cells were cultured in pro-osteoclastogenic media until osteoclast differentiation (5 to 7 days), and then media was replaced with specific media for 72 hours. In particular, we used DMEM medium supplemented with penicillin [20 U/mL] and streptomycin [100 mg/mL], 10% FBS, buffered at pH 7.4 with 3.7 g/liter NaHCO3, plus 20 mM glucose (complete glucose medium), or 20 mM galactose (Sigma) (complete galactose medium), or with complete galactose medium supplemented with rotenone (10 nM; Sigma). Supernatants were collected after 10 days and the fraction of collagen Type I degradation quantified by the emission of Europium-labelled collagen fragments via time resolved fluorescence (Infinite® 200 PRO, Tecan, exc. 340 nm, ems. 615 nm).

3.4 SDS-PAGE and immunoblotting

PBMC were seeded on cell culture dishes, and maintained in pro-osteoclastogenic media or control media until osteoclast differentiation was obtained. When multinucleated TRAP+ cells were formed (around 7 days), cells were lysed with RIPA buffer [Tris pH 7.6 50 mM, NaCl 150 mM, Triton-X 100 5%, sodium deoxycholate 0.25%, EGTA pH 8 1 mM, NaF 1 mM] (Sigma) containing protease and phosphatase inhibitor cocktails (Roche). Protein lysates were subjected to reducing SDS-PAGE on polyacrylamide gel and transferred to nitrocellulose membrane (Thermo Fisher Scientific). Membranes were stained with Ponceau red (Sigma) to confirm equal amount protein loading. Blots were probed with MitoProýle Total OxPhos human antibody Cocktail (1:300; ab110411, Abcam), with MCT1 (1:1000, Chemicon, AB3538P), with ACTB

(1:1000, Cell signalling, 4970) and with anti-Heat Shock Protein 60 kDa (HSP60, 1:2000; HPA001523, Sigma), followed with horseradish peroxidase-conjugated anti-mouse and anti-rabbit (GE Healthcare). To detect HSP60 and ACTB within the same blot, nitrocellulose membranes were stripped with Restore Western Blot Stripping buffer (Thermo Fisher Scientiýc), and reprobed. The reaction was revealed by a chemiluminescence substrate (ECL Western Blotting Detection Reagents, GE Healthcare). The signal from each band was quantiýed by dedicated software for densitometric evaluation (VisionWorksLS Analysis Software, Biospectrum, UVP). Results are representative of 4 independent experiments.

3.5 Microscopy analyses

3.5.1 Immunofluorescence analyses

Immunofluorescence assays were performed on PBMC cultured on glass coverslips with pro-osteoclastogenic media or control media. Cells were fixed in 2% paraformaldehyde. Permeabilization was performed with 0.5% Triton X-100 in HEPES and blocked with 1% BSA. We used anti-mitochondria MAb against the surface of intact mitochondria (clone 113-1, MAB1273, Merck Millipore, 1:50). As a secondary antibody we used anti-mouse or anti-rabbit antibodies Alexa Fluor 488 nm (Life Technologies). Nuclei were stained with Hoechst 33258. Mitochondrial mass index was quantified as the ratio of the area with a fluorescent signal with the total area of the single cell by using NIS Element image software BR4.00.00 (Nikon). 28 different random cells were counted. Mitochondria networks were observed by confocal microscope (Nikon TI-E).

3.5.2 Immunohistochemistry

Paraffin sections of giant-cell tumor of bone were stained with MCT1 antibody.

Sections were dewaxed, rehydrated through graded ethanol series, and antigen retrieval was performed with 10 mM citrate buffer, pH 6.0 for about 10 minutes using a microwave. The cooled sections were blocked with 3% hydrogen peroxide and next incubated with 5% BSA for 1 hour, followed by overnight incubation with anti-MCT1 antibody (HPA003324, 1:100, Sigma) at 4°C. Biotinylated secondary antibodies followed by streptavidin-horseradish peroxidase conjugated were from Dako. Immunoreactivity was revealed with the DAB solution (Dako). Sections were counterstained with hematoxylin.

3.5.3 Electron microscopy

CD14+ cells were isolated from the mononuclear cell population obtained from buffy coats with the method described above, and according to a protocol previously defined [142]. Briefly, we used an immunomagnetic cell separation technique (MACS, Miltenyi Biotech). Cells were washed with MACS buffer (PBS pH 7.2 supplemented with 0.5 % bovine serum albumin and 2 mM ethylene diamine tetracetic acid), and clumps were removed by passing cells through a 30 mm pre-ýlter. Cells were then centrifuged at 400 g. The cell pellet was resuspended in MACS buffer and counted. 107 cells were mixed with anti-CD14 MACS antibody-coated microbeads, and incubated at room temperature. The cell suspension was applied to an LS-positive selection column previously washed with MACS buffer, and placed in a magnetic separation unit. The column was rinsed and removed from the magnetic separation unit, and positive bound cells were þushed. The collected cell population was then used for ultrastructure evaluation. Pellet of CD14+ cells from PBMC and glass-adherent osteoclasts were fixed in 2.5% glutaraldehyde in 0.1 M cacodylate buffer, pH 7.4, for 1 hour, postfixed with 1% osmium tetroxide (Electron Microscopy Science), dehydrated in a graded series of ethanol, and embedded in Epon

(Electron Microscopy Science). The embedded samples were sectioned on ultramicrotome (Ultracut E, Richert-Jung, Leica Microsystem). Thin sections (90 nm thick) were collected on 300 mesh nickel grids and stained with uranyl acetate (Electron Microscopy Science) and lead citrate. Mitochondria were observed by using a Zeiss EM 109 apparatus (Zeiss). Images were captured with Nikon digital camera Dmx 170 1200F and ACT-1 software.

3.6 Molecular biology procedures

3.6.1 Total RNA isolation and cDNA synthesis

Total RNA was extracted from CSC and native cells from all the different histotypes included in the study, and from osteoclasts, control cells, MDA-MB-231, MDA-MB-231 bone met, MSC and osteoblast, by using the NucleoSpin RNA II (Macherey-Nagel, Düren, Germany). On-column DNase digestion was performed following manufacturerôs instructions. The total RNA purity was quantified using a Nanodrop Spectrophotometer (NanoDrop Technologies). Total RNA (0.5 εg) were reverse-transcribed into cDNA in 20 εl final volume, using MuLV Reverse Transcriptase and RNase inhibitor (Applied Biosystems, Foster City, Ca, USA). First-strand cDNA was synthesized using random hexamers. For each sample, 3 biological replicates were processed.

3.6.2 qRT-PCR

qRT-PCR was performed by using a Light Cycler instrument and the Universal Probe Library system (Roche Applied Science, Monza, Italy). Probe and primers were selected by using a web-based assay design software (ProbeFinder https://www.roche-applied-science.com), and were further controlled using Oligo Primer Analysis Software. Only primers spanning an exon-exon junction and producing a PCR amplificate with length between 70 and 150 base pairs

were selected. All the primers designed were analyzed by BLAST to verify their specificity (National Center for Biotechnology Information). All cDNA were diluted 1:10, and 10 εl were used as template and included in a 20 εl of total volume of qRT-PCR reaction. The protocol of ampliýcation was: 95°C for 10 min; 95°C for 10 s, 60°C for 30 s, and 72°C for 1 s for 45 cycles; 40°C for 30 s. Each assay included a blank. Table 1 provides a summary of all the housekeeping genes (HKG), primer sequences, and probes included in this study.

Table 3.1. Candidate HKG genes

Gene	Full name	Function	Accession Number	Primers	Probe
18S rRNA	18S ribosomal RNA	Structural RNA for the small component of eukaryotic cytoplasmic ribosomes.	X03205.1	F=gcaattattccccatgaacg R=gggacttaatcaacgcaagc	48
ACTB	Actin, beta	Cytoskeletal structural protein	NM_001101.2	F=ccaccgcgagaagatga R=ccagaggcgtacagggatag	64
B2M	Beta-2-microglobulin	Component of the class I major histocompatibility complex (MHC)	NM_004048.2	F=ttctggcctggaggctatc R=tcaggaaatttgactttccattc	42
G6PD	Glucose-6-phosphate dehydrogenase	Produces pentose sugars for nucleic acid synthesis and main producer of NADPH reducing power	M24470.1|M24470	F=gaagggccacatcatctctg R=atctgctccagttccaaagg	75
GAPDH	Glyceraldehyde 3-phosphate	Oxidoreductase in glycolysis and gluconeogenesis	NM_002046.3	F=agccacatcgctcagacac R=gcccaatacgaccaaatcc	60

	dehydrogenase				
GUSB	Beta-glucuronidase	Hyrolase that degrades glycosaminoglycans	M15182.1| M15182	F=cgccctgcctatctgtattc R=tccccacagggagtgtgtag	57
HMBS	Hydroxymethylbilane synthase	Third enzyme in the heme biosynthetic pathway	NM_000190.3	F=tgtggtgggaaccagctc R=tgttgaggtttccccgaat	26
HPRT1	Hypoxanthine phosphoribosyltransferase 1	Purine synthesis in salvage pathway	M31642.1| M31642	F=tgaccttgatttattttgcataccc R=cgagcaagacgttcagtcct	73
PGK1	Phosphoglycerate kinase 1	Transferase in glycolysis and gluconeogenesis	NM_000291.3	F=ggagaacctccgctttcat R=gctggctcggctttaacc	69
PPIA	Peptidylprolyl isomerase A (cyclophilin A)	Isomerase involved in the cis-trans isomerization of peptide bonds in oligopeptides	NM_021130.3	F=atgctggacccaacacaaat R=tctttcactttgccaaacacc	48
RPL13a	Ribosomal protein L13a	Structural component of the large 60S ribosomal subunit	NM_012423.3	F=caagcggatgaacaccaac R=tgtggggcagcatacctc	28
SDHA	Succinate dehydrogenase complex, subunit A, flavoprotein (Fp)	Electron transporter in the TCA cycle and respiratory chain	NM_004168.2	F=ggacctggttgtctttggtc R=ccagcgtttggtttaattgg	80
TBP	TATA-binding protein	General RNA polymerase II transcription factor	NM_001172085.1	F=ttgggttttccagctaagttctt R=ccaggaaataactctggctca	24
TUBB	Tubulin, beta	Major constituent of microtubules	NM_178014.2	F=ataccttgaggcgagcaaaa	64

	class I			R=tcactgatcacctcccagaac	
YWHAZ	Tyrosine 3-monooxygenase/tryptophan 5-monooxygenase activation protein zeta polypeptide	Belongs to the 14-3-3 family of protein which mediate signal transduction	NM_003406.3	F=ccgttacttggctgaggttg R=tgcttgttgtgactgatcgac	9

To evaluate MCTs expression by cells of the bone metastatic microenvironment, MCT1 (NM_003051.3) and MCT4 (NM_001206952) were analyzed by using the following primers: MCT1-F 5ô-ggattggtgaccattgtgg-3ô, MCT1-R 5ô-catgtcattgagccgaccta-3ô. MCT4-F 5ô- gagtttgggatcggctacag-3ô, MCT4-R 5ô-cggttcacgcacacactg-3ô. The relative expression of MCT1 and MCT4 were normalized by the reference gene ACTB for MDA-MB-231 and MDA-MB-231 bone met, by TBP for osteoclasts and precursors cells, or by PPIA for MSC and osteoblast [143]. Relative expression calculation was performed using the qpqpCt model [144].

For the evaluation of the expression of stemness markers of CSC, c-Myc (NM_002467.4), KLF4 (NM_004235.4), Nanog (NM_0248695.2) and OCT3/4 (NM_002701.4) were analysed, and the following primers were used: c-Myc-F 5ô-gctgcttagacgctggattt-3ô, c-Myc-R 5ô-taacgttgaggggcatcg-3ô, probe 66; KLF4-F 5ô-ccatctttctccacgttcg-3ô, KLF4-R 5ô-agtcgcttcatgtgggagag-3ô, probe 7;. Nanog-F 5ô-ATGCCTCACACGGAGACTGT-3ô, Nanog-R 5ô-AGGGCTGTCCTGAATAAGCA-3, probe 69; OCT3/4-F 5ô-CTTCGCAAGCCCTCATTTC-3ô, OCT3/4-R 5ô-

GAGAAGGCGAAATCCGAAG-3ô, probe 60. For the purpose of normalization, the relative expression of KLF4, c-Myc, Nanog and OCT3/4 were normalized by the reference gene ACTB or for the geometric average of YWHAZ and GAPDH for CSC and native cells from MG-63, or for the geometric average of PPIA and HMBS for CSC and native cells from ACHN and MDA-MB-231. The relative expression of the stem cell markers was calculated using the qpqpCt model [144].

3.7 Illumina Genome Analyzer sequencing and data analysis

A deep sequencing analysis of MG-63, HOS, and Saos-2 OS cell models was performed to compare the global transcriptional expression of CSC to the respective native cells, in order to select a panel of stable HKG for qRT-PCR analysis. Briefly, total RNA was collected from the cell lysate in acid guanidinium thiocyanate-phenol-chloroform [145]. The total RNA was quantified by Bioanalyzer (Agilent, Santa Clara, CA) following the manufacturer's instructions. RIN (RNA Integrity Number) and A260/A280 ratio of the prepared total RNA were all 10, and over 1.8, respectively. The library of template molecules for high throughput DNA sequencing was converted from the total RNA using TruSeq RNA Sample Prep Kit v2 (Illumina, San Diego, CA), following the manufacturer's protocol. The library was also quantified with Bioanalyzer (Agilent), following the manufacturer's instruction. The library (7 pM) was subjected to cluster amplification on a Single Read Flow Cell v4 with a cluster generation instrument (Illumina). Sequencing was performed on a Genome Analyzer GAIIx for 70 cycles using Cycle Sequencing v4 regents (Illumina). Human genome build 19 (hg19) were downloaded from University of California, Santa Cruz genome browser (http://genome.ucsc.edu/). Image analysis and base calling were performed using Off-Line Basecaller Software

1.6 (Illumina). Reads were aligned using ELAND v2 of CASAVA Software 1.7 with the sequence data sets. Transcript coverage for every gene locus was calculated from the total number passing filter reads that mapped, by ELAND-RNA, to exons. These analyses were performed using default parameters. The data were viewed using Genome Studio Software (Illumina). The advanced analysis for quantification with Quantile normalization algorithm was performed using Avadis NGS software (version1.5, Strand Scientific Intelligence Inc., San Francisco, CA).

3.8 Software for housekeeping gene stability analyses

3.8.1 NormFinder analysis

NormFinder program is a VBA applet [146] based on a variance estimation approach, which ranks the candidate HKG based on their stability evaluation, and assigns a stability value to each candidate gene using a model-based approach. In agreement with NormFinder requirements, the Ct values were transformed in relative quantity, using the lowest Ct value as calibrator. According to the analysis, the lowest stability value was top ranked. We grouped all the data in 3 different clusters: 1) all data from CSC of different tumors; 2) all data from native cells of different tumors; 3) all data from different tumors with CSC and native cells pooled together. For the third group of data, in addition to CSC and native cells obtained from all tumors pooled together, we also considered CSC and native cells obtained from the single tumor type, from sarcoma or from carcinoma. All results were obtained from 3 sets of replicates.

3.8.2 GeNorm analysis

GeNorm v. 3.0 [147] available in qbase+ [148] (Biogazelle, Ghent University, Belgium, http://www.qbaseplus.com) was used to evaluate the stability of

candidate HKG. GeNorm calculates all the possible average pairwise variation between the candidate genes and provides a measure of the expression stability (M) of each gene. An M-value below 1.5 indicates stable HKG. The candidate reference gene with the lowest M value was considered to have the most stable expression. GeNorm ranks candidate reference genes on the basis of their stability of expression, and performing stepwise exclusion of the gene with the highest M-value (the least stable expressed gene), and recalculates M-values for the remaining genes. We use also GeNorm to verify if a single HKG is sufficient for an adequate normalization. Indeed, GeNorm provides the optimal number of reference genes required for accurate normalization. V values below the cut-off value 0.15 indicated the optimal number of genes required for data normalization. Similarly to the analysis performed with NormFinder, we grouped all the data and the results in 3 different clusters. All results were obtained from 3 sets of replicates.

3.8.3 Coefficient of variation analysis

Gene expression stability evaluated by the coefficient of variation (CV) was calculated by dividing the standard deviation (SD) of threshold cycles (Ct) by the mean Ct value. As in the analysis performed with NormFinder and GeNorm, we grouped all the data in 3 different clusters, and the results were obtained from 3 sets of replicates.

3.8.4 Rank aggregation

The analyses performed by the three described methods showed some differences in the stability rank of the HKG. Therefore, we identified the most stable genes by considering the lowest value of the mathematic average of the NormFinder, geNorm and CV method ranks for every single gene.

3.9 Statistical analyses

Statistical analysis was performed using GraphPad Prism version 5.00 for Windows (GraphPad Software, San Diego California USA, www.graphpad.com). Due to low number of observations, data were considered as not normally distributed, and nonparametric Mann-Whitney U test were used to evaluate the differences. The Spearman Rank correlation test was used for the correlation analyses. Results were reported as mean ± standard error of mean (SEM). Standard deviation (SD) of delta cycle threshold (qpCt) values was calculated as pooled standard deviation (SDpooled). HKG expression variation in CSC and native cells was evaluated with the paired Wilcoxon signed-rank test. For all the analyses, differences were considered signiýcant with a *p*-values Ò0.05.

4. RESULTS

To evaluate the complex interaction between the cells of the bone metastatic microenvironment underlying the formation and activation of lytic lesions, we focused on the study of metabolic adaptation that occurs in the bone microenvironment. The result chapter is divided in three sections. In the first section I characterized the basal metabolism of human osteoclast cells, the main actors of bone resorption in osteolytic metastases, during osteoclast formation and activity. In the second section I analyzed the role of lactate, an energy-rich metabolite produced by the glycolytic metabolism of metastatic breast carcinoma cells, on osteoclast cells. In the third section, with the aim to lay the groundwork to future analyses on the role of CSC in bone metastases, I validated the most stable housekeeping genes for the comparison CSC with respect to native adherent tumor cells (this section is modified from Lemma S. et al, 2016. PLoS ONE 11(2): e0149481).

Section 1: Energy metabolism is finely tuned during osteoclast formation and function

4.1.1 Mitochondrial mass increases along with the osteoclast differentiation process

Human osteoclasts were obtained from PBMC treated with the pro-osteoclastogenic media containing RANKL and M-CSF. At 2 days, undifferentiated mononuclear precursors were observed that, after 7 days of culture, fused together to form TRAP+ multinucleated osteoclasts. The number of fully differentiated osteoclasts was maintained until 14 days of cell culture (Fig. 4.1A).

In mature osteoclasts, the mitochondrial mass was markedly and significantly increased with respect of precursor cells at 2 days of culture (Fig 4.1B-C ***p<0.0001). We also found a positive correlation between mitochondrial mass and both the number of nuclei and the cell size (Fig. 4.1D, R2=0.9122, *p = 0.0178).

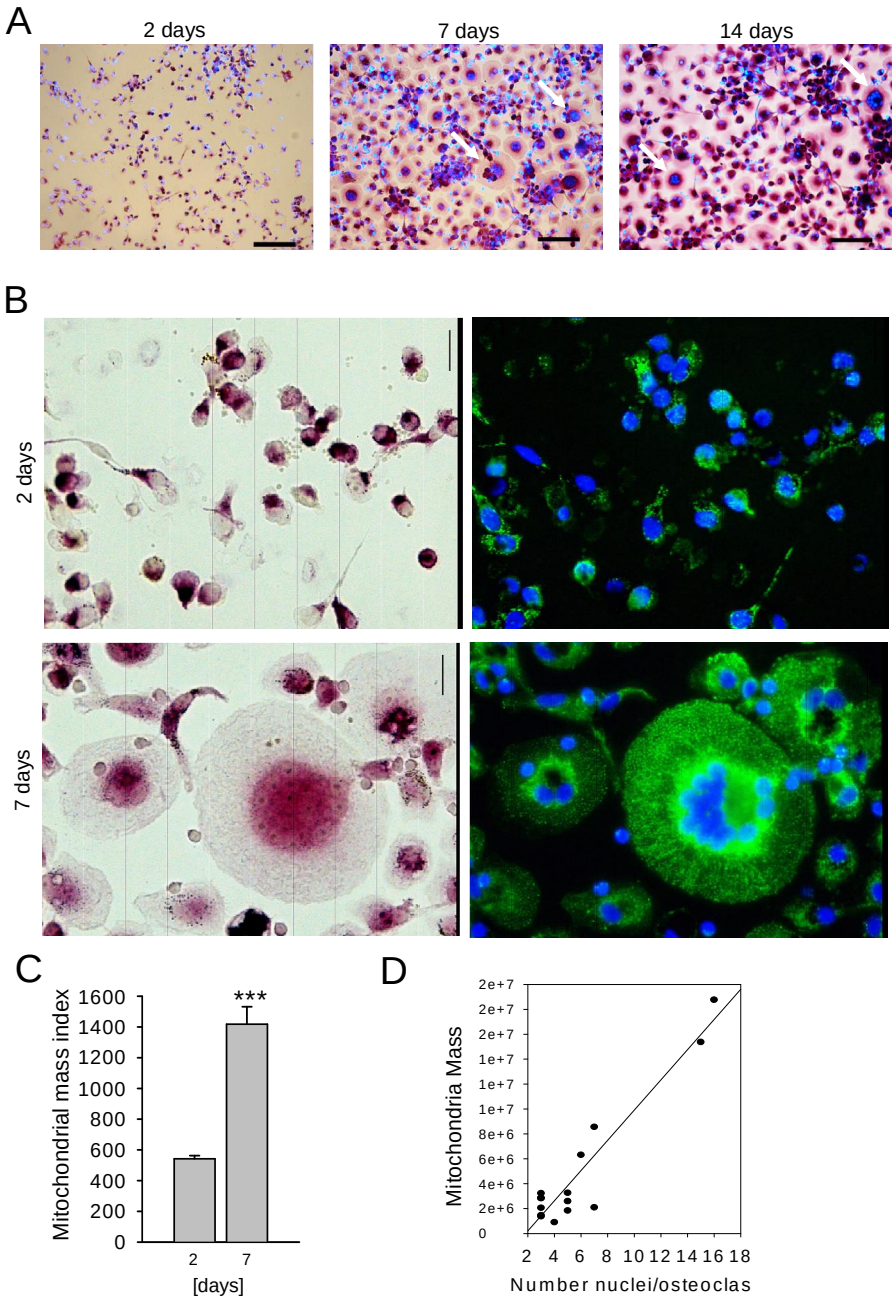

Figure 4.1. Human osteoclasts display an increased mitochondrial mass. (A) TRAP and

nuclei staining of osteoclast cultures at 2, 7 and 14 days (white arrows show multinucleated TRAP+ cells); (B) Representative images of immunofluorescence with anti-mitochondria antibody (right panel) of osteoclast precursors at 2 days of culture (upper panel) and mature osteoclasts at 7 days of culture (bottom panel). The osteoclast phenotype of the observed cells were confirmed by TRAP staining and multinuclearity (left panel). Original magnification, 40x. Scale bar 20 ε m; (C) Mitochondrial mass index during osteoclastogenesis (***$p<0.0001$, n=28); (D) Mitochondrial mass is directly correlated with the number of nuclei for cell ($R2=0.9122$, n=9) and with osteoclast size (n=15). Only cells with 3 or more nuclei were considered in the analyses.

Then, mitochondria were examined at different osteoclast differentiation phases by ultrastructural analysis. Osteoclasts derive largely from CD14-positive cells, therefore, to obtain a pure population of osteoclast precursors, we used CD14-positive monocyte isolated from PBMC as model of osteoclast precursor cells. Both CD14-positive cells and osteoclast were characterized by a high number of mitochondria in the cytosol. Osteoclasts showed large mitochondria (Fig. 4.2, left panels), with a complex organization of cristal membranes (Fig.4.2, right panels) respect to CD14-positive precursors.

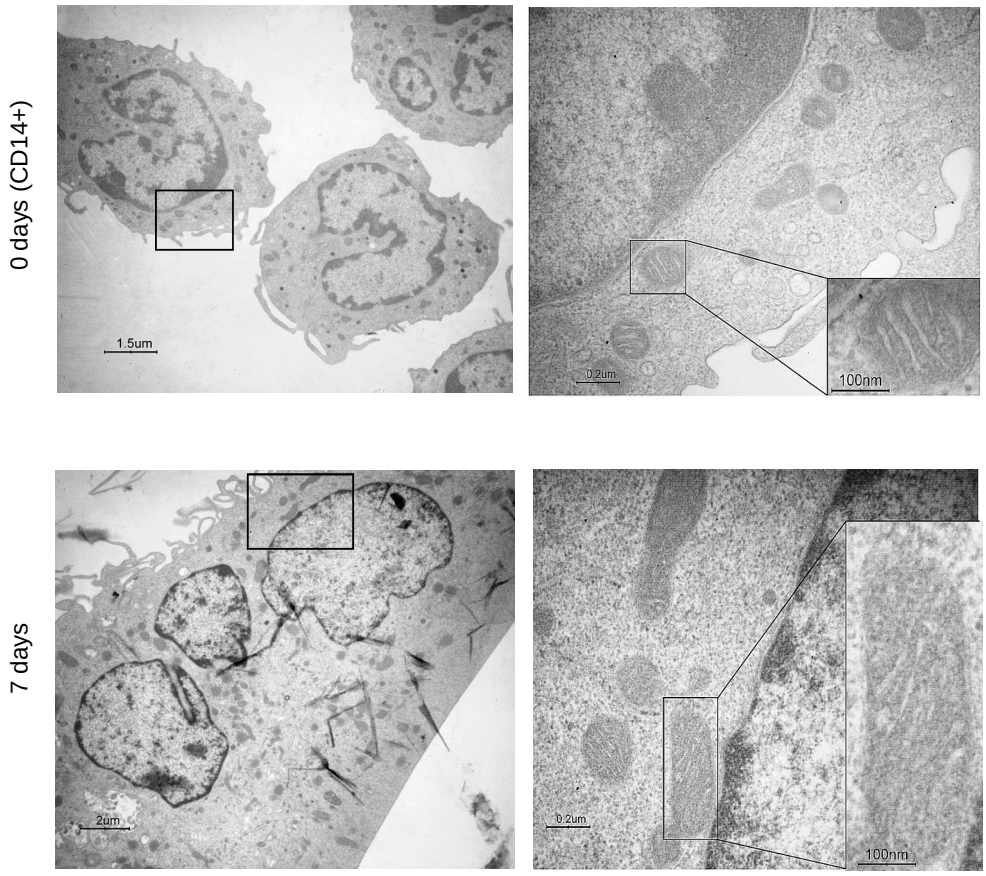

Figure 4.2. Ultrastructural analysis of mitochondria. Representative images from monocytic precursors (CD14-positive cells) isolated from PBMC (upper panels) and mature osteoclasts (7 days, lower panels). Scale bars: 1.5-2 εm on the left, 0.2 εm on the right, 100 nm for magnification.

The overall morphology of the entire mitochondrial network of osteoclast was observed by confocal microscopy. In human osteoclasts, mitochondria appeared as a reticulum clustered in the perinuclear region (Fig. 4.3A) that extended outward into the peripheral basal domain of the cell, where appeared to be elaborately interconnected and ramified (Fig 4.3B). The mitochondrial reticulum was made up of tubular structures that localized perinuclear in the apical domain of the cells and branch out to the lower side of the cells, where it organized as elongated tubular structure close to the basal domain of the osteoclast (Fig. 4.4).

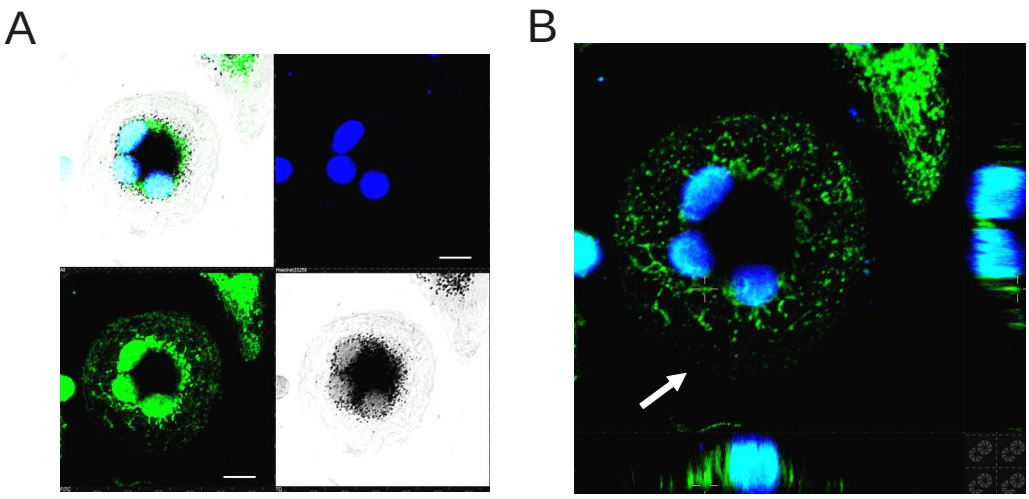

Figure 4.3. Mitochondria of mature osteoclast are organized in tubular structure. (A) Osteoclasts were stained with an anti-mitochondria antibody, and analyzed by confocal microscopy. The presence of mature osteoclasts was revealed by positivity to TRAP staining and the presence of more than 3 nuclei. Mitochondria clusters in the perinuclear region. (B) Detail of the tubular structure organization of mitochondria in osteoclasts.

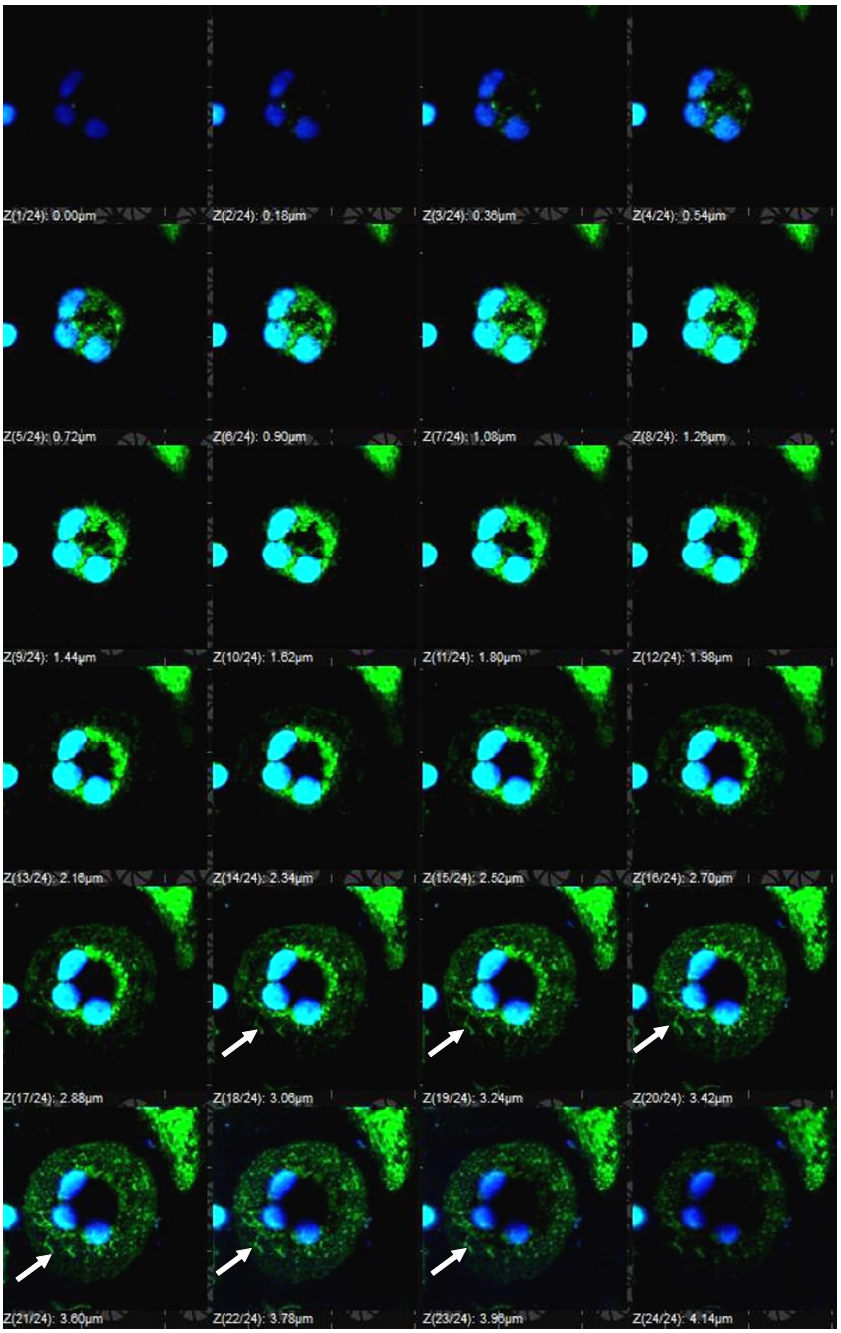

Figure 4.4. Mitochondria network in mature osteoclast. Note that tubular structure of mitochondria localized in the basal domain of osteoclast.

4.1.2 Mitochondrial energy metabolism increases during osteoclast differentiation

Since mitochondrial biogenesis is usually associated with increased OxPhos, we analyzed the expression of OxPhos complex subunits,

total intracellular ATP pool, and the respiration rate in osteoclasts in respect to control cells. As control cells we used mononuclear precursors cultured for the same number of days and not treated with growth factors. Western blot analyses revealed that osteoclasts express significantly higher levels of complexes I, II, III and V with respect to control cells (Fig 4.5A-B), and produced higher levels of intracellular ATP with respect to control cells (Fig 4.5C).

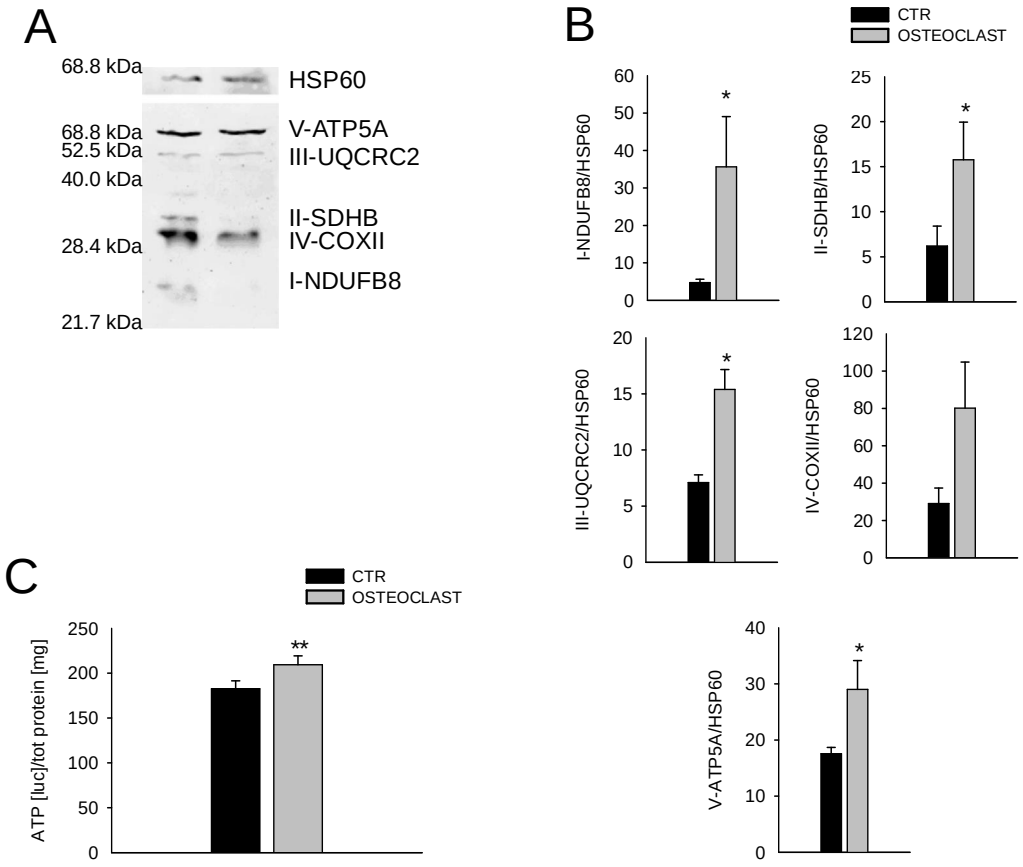

Figure 4.5. Expression of enzymes of the respiratory chain and total ATP intracellular content. (A) Immunoblot analysis of Complex I (I-NDUFB8), complex II (II-SDHB), complex III (III-UQCRC2), complex IV (IV-COXII) and complex V (V-ATP5A) of the electron transport chain of osteoclast and control cells. HSP60 immunoblot was used for normalization. (B) The plots reports the densitometric quantitation (ratio of each protein:HSP60). Note that I-NDUFB8, II-SDHB, III-UQCRC2, and V-ATP5A were upregulated in osteoclast. *p<0.05, nÓ3. (C) Total intracellular ATP was increased in

osteoclast with respect to control cells. Results were normalized to total protein content. **p<0.01, n=10.

As a means of verification of the increased OxPhos metabolism in human osteoclasts, we evaluated metabolic changes that occur during osteoclastogenesis by analyzing oxygen consumption rate (OCR) and extracellular acidification rate (ECAR) of living precursors and mature osteoclast (i.e. 7-14 days of differentiation). We found that ECAR values were lower in cells treated with osteoclast differentiating factors with respect to untreated cells, whereas OCR values were higher in osteoclast then in control cells, except for precursors cells (Fig. 4.6A-B). To confirm the high mitochondrial activity, we measured the oligomycin-sensitive OCR (mtOCR), the ATP coupling efficiency, and the glycolytic efficiency of mature osteoclast cells. We found a significantly higher mtOCR and a low glycolytic efficiency, with a tendency in higher ATPcoupling and lower ECAR in osteoclasts with respect to control cells (Fig. 6C-D).

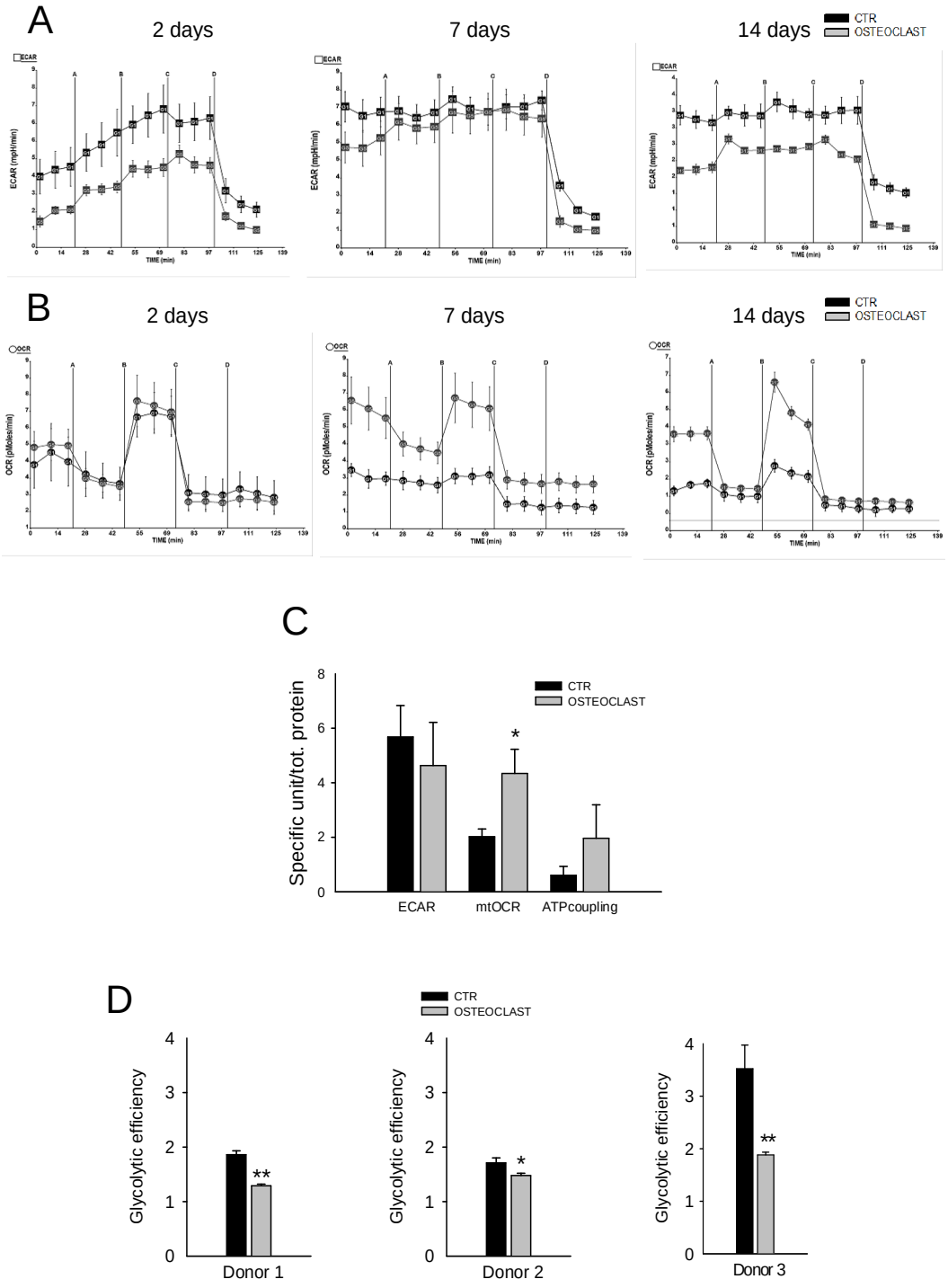

Figure 4.6. Energetic metabolism during osteoclast differentiation. Osteoclasts and immature cells were cultured for 14 days, and baseline ECAR and OCR were measured using the Seahorse Flux Analyzer. Typically, after the incubation with osteoclast differentiation, osteoclasts are formed starting from day 7. ECAR, extracellular acidification rate; OCR, oxygen consumption rate; mtOCR, mitochondrial OCR. Graphs showed the ECAR (A) and

OCR measurements (B) at different time points of a representative osteoclast culture obtained from a single donor (A, B, C, D vertical lines correspond to the time of injection of oligomycin, FCCP, rotenone and antimycin A, 2-deoxy-glucose 100 mM respectively); (C) ECAR, mtOCR, and ATP coupling values of cells treated with osteoclast differentiating factors, or not treated, at 7 days of cultures. Average of different cultures obtained from different donors. Mean ±SE (*$p<0.05$, n=3); (D) Glycolytic efficiency (glucose consumption/lactate production ratio) Each graph represents the results obtained for each individual culture obtained from 3 different donors. *$p<0.05$, **$p<0.01$, n=5. All the results were normalized by total protein.

4.1.3 Energetic metabolism during bone resorption

After confirming that the energetic demand for osteoclast formation is largely fulfilled by the oxidative metabolism, we wondered about the metabolic profile of osteoclast activated to resorption. To investigate if osteoclast activity is mainly driven by glycolysis or OxPhos, mature osteoclasts were exposed to complete cell culture medium containing only glucose or only galactose as energetic fuel [149] and seeded on a layer of collagenous matrix. Glucose promotes glycolysis, whereas galactose force cells to depend on OxPhos to generate sufficient ATP by reducing the rate of glycolysis [150]. We found that, when mature osteoclasts were exposed to glucose, type I collagen degradation activity was significantly increased with respect to galactose (Fig 4.7A). Moreover, the combination of galactose with rotenone that inhibits complex I of electron transport chain significantly increased collagen Type I degradation activity with respect to cell cultures containing only galactose in the medium (Fig 4.7B). Notably, to evaluate the resorption activity of osteoclasts we used a not toxic concentration of rotenone (10 nM) (data not shown). Our results demonstrate that glycolysis is the key energetic pathway driving the resorption activity of mature osteoclasts, while oxidative metabolism is maintained to support other simultaneous cellular functions.

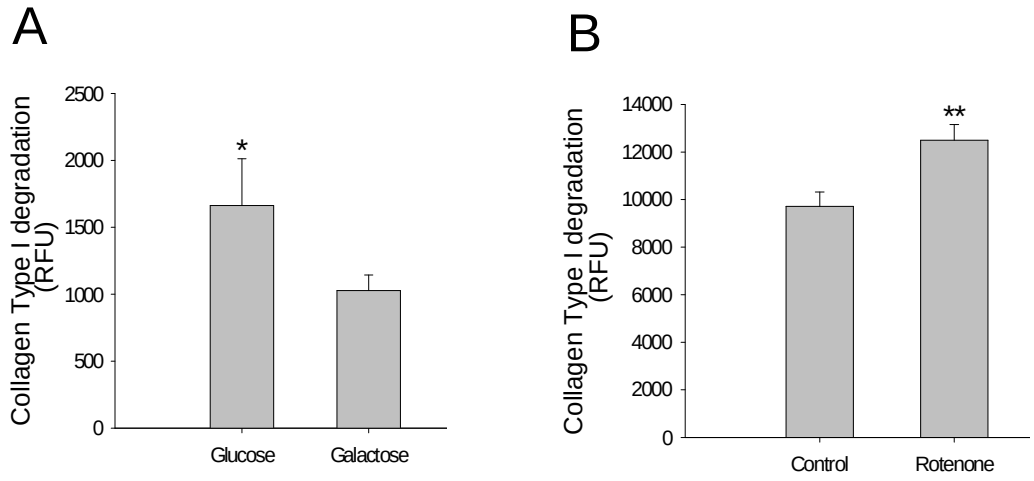

Figure 4.7. Glycolysis drives the activity of human osteoclasts. (A) Type I collagen degradation activity of osteoclast is regulated by glucose metabolism. *p<0.05, n=4. (B) Inhibition of the mitochondrial complex I with rotenone 10 nM in galactose media increased the type I collagen degradation activity of osteoclast. **p<0.01, n=8.

Section 2: Lactate fuels the basal metabolism of human osteoclasts

4.2.1 Expression of MCT1 increases during osteoclastogenesis

The bone metastatic microenvironment is a cellular matrix composed of bone matrix and several cellular elements, including tumor cells that spread to the bone, bone resident cells and stromal cells. In the context of lytic bone metastases, osteoclast actively resorbs bone, thereby playing a primary role in the pathogenesis of bone metastases. To study the role of lactate and of MCT shuttles in the metastasis microenvironment, I first focused the analyses on MCT expression in osteoclast cells. Western blot analyses revealed that osteoclasts express high levels of MCT1, and, most importantly, the expression of MCT1 increases during the differentiation of osteoclasts (Fig. 4.8A-B). MCT1 expression increased during osteoclastogenesis at the mRNA level as well, as

confirmed by qRT-PCR analyses (Fig. 4.8C), whereas MCT4 expression was lower both in precursors and mature osteoclasts (Fig. 4.8C). Notably, mature osteoclasts were able to take up ^{14}C-sodium lactate in a dose-dependent manner (Fig. 4.8D). To assess if the high MCT1 expression observed in human osteoclast *in vitro* also occurs *in vivo*, we analysed the expression of MCT1 in giant-cell tumor of bone (GCT), a benign adult human tumor characterized by the presence of multinucleated osteoclast-like cells [142]. The immunohistochemistry analyses on paraffin section demonstrated that MCT1 was highly expressed in osteoclasts, whereas it is lower expressed by other bone-resident cells (Fig. 4.8E).

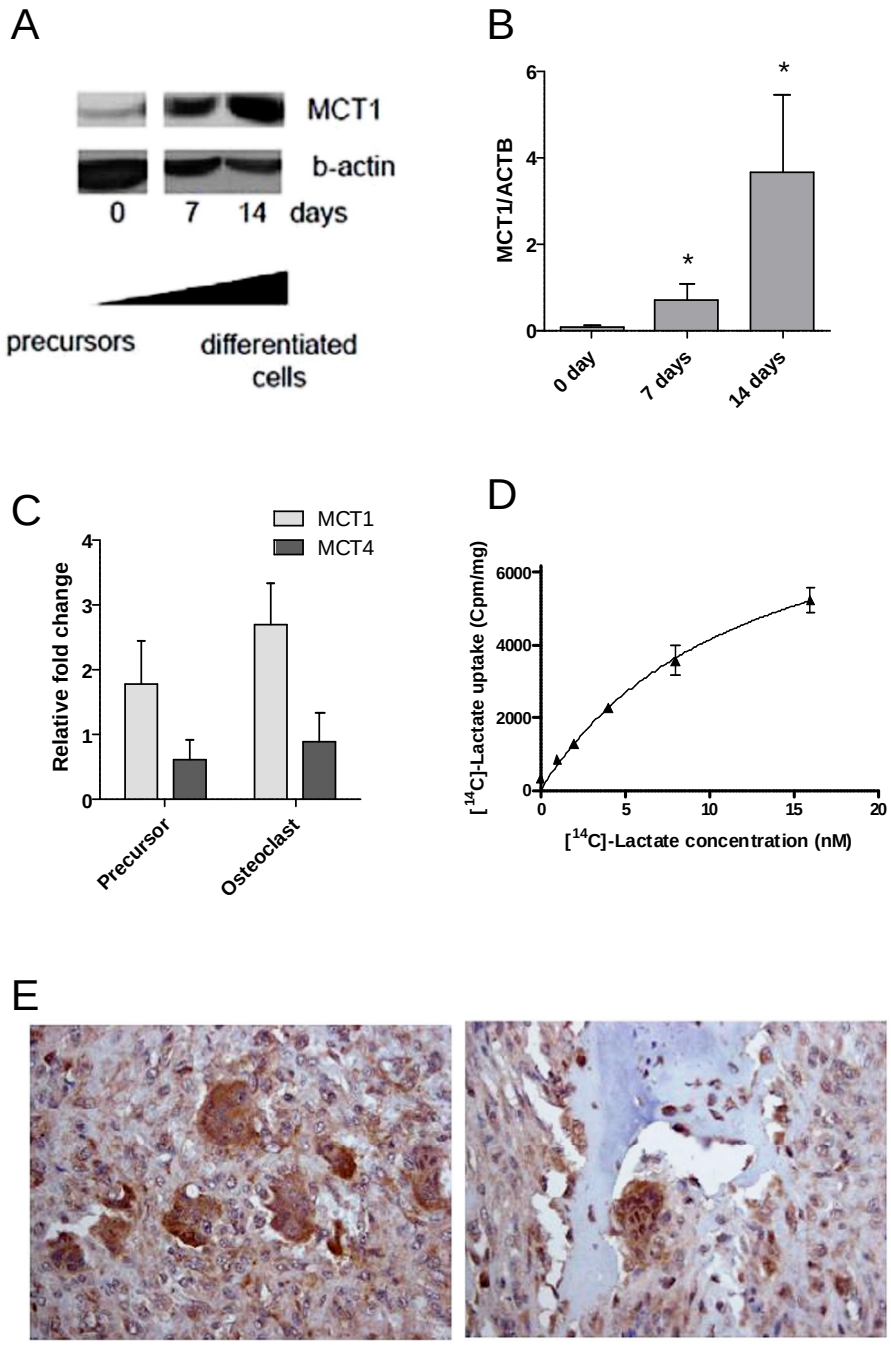

Figure 4.8. MCT expression increases during osteoclastogenesis and is relevant in giant-cell tumor of bone. (A) Immunoblot analysis of MCT1 in precursor cells (0 days) and in mature osteoclast (7-14 days of differentiation). ACTB immunoblot was used for normalization. (B) The plot report the densitometric quantitation of MCT1:ACTB. Note that MCT1 increases during osteoclast differentiation from precursors cells. *$p<0.05$, n=3. (C) MCT1 and MCT4 mRNA expression in precursor and mature osteoclast. Normalization to TBP. (D) ^{14}C-Lactate uptake in mature osteoclasts. Result is normalised to total protein

(mg/well), n=4. (E) MCT1 immunohistochemistry was performed on human Giant-cell tumor of bone (GCT). Note that osteoclast are strongly stained for MCT1 (brown), while other bone-resident cells are poorly stained. Original magnification 20x.

4.2.2 Cells of bone metastatic microenvironment express high levels of MCT4

The expression of MCT shuttles by the cells of the bone metastatic microenvironment were analyzed in breast carcinoma cell lines, in MSC from bone marrow, and in osteoblast differentiated from MSC. As cellular model of breast carcinoma cells we used MDA-MB-231 and MDA-MB-231 bone met, a clone prone to form bone metastases when injected intracardiacally in mice [141]. The qRT-PCR analyses of MCT1 and MCT4 revealed a significantly higher expression of MCT4 with respect to MCT1 in the two breast carcinoma cell lines, and in MSC, whereas osteoblast present low levels of both MCT shuttles (Fig. 4.9A,C). We also found that breast carcinoma cell lines produced and released about 10 mM lactate in supernatant, thereby confirming its capacity to export lactate in the tumor microenvironment (Fig. 4.9B).

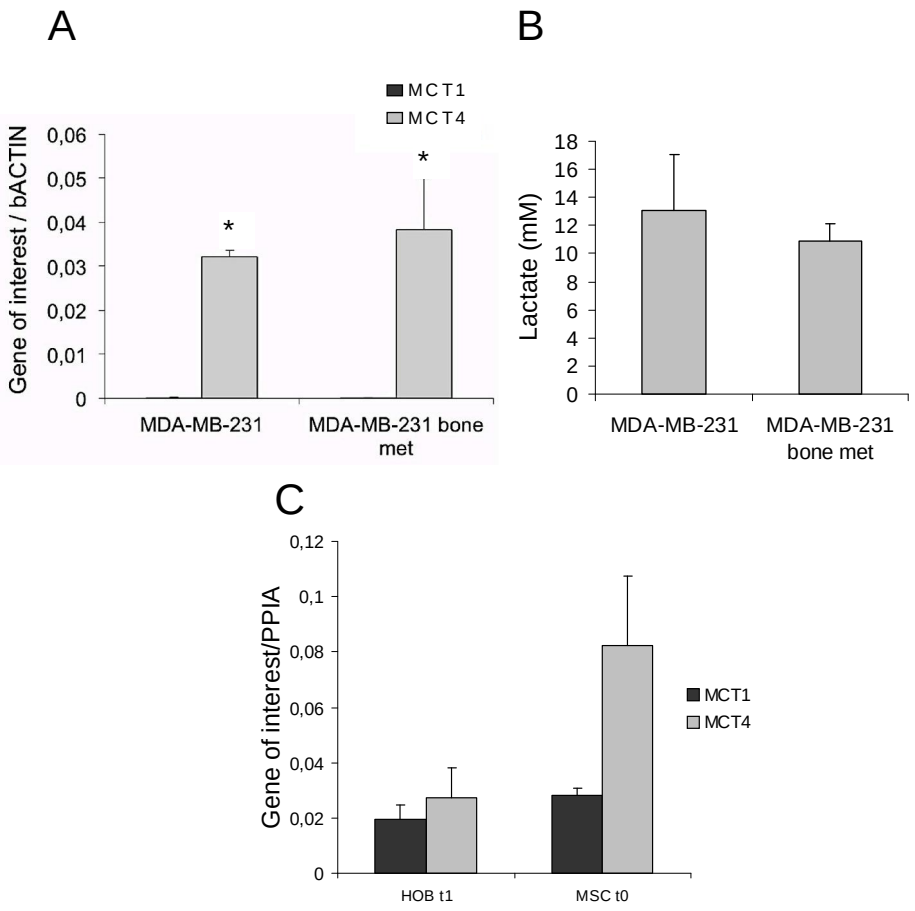

Figure 4.9. MCT expression in breast carcinoma cells, MSC and osteoblasts. (A) MCT1 and MCT4 mRNA expression in MDA-MB-231 and MDA-MB-231bone-met cells. Normalization to ACTB. *p<0.05, n=3. (B) Lactate production by MDA-MB-231 and MDA-MB-231bone-met cells was measured from cell supernatants. Results were normalised by total protein. p=ns, n=3. (C) MCT1 and MCT4 mRNA expression in bone marrow MSC (MSC t0) and human osteoblasts (HOB t1) derived from MSC. Normalization to PPIA. p=ns, n=5.

4.2.3 Lactate fuels the basal metabolism of human osteoclasts

Considering that osteoclast rely on OxPhos as main source for energy production, that MDA-MB-231 cells release high levels of lactate, and that osteoclasts are able to uptake extracellular lactate, we evaluated the effect of lactate (10 mM) on the oxidative metabolism of human osteoclasts. Metabolism of living osteoclasts was evaluated by mitochondrial OCR, ATP coupling of

mitochondria, and ECAR. We found that lactate significantly increased the oxidative metabolism of osteoclasts (Fig 4.10A-B), without affecting ECAR (Fig. 4.10C), and that lactate significantly decreased the glycolytic efficiency of osteoclast with respect to not treated cells (Fig 4.10D). We confirmed that mitochondria metabolism is increased in the presence of lactate by using the fluorescent probe JC-1, a vital dye that accumulates in mitochondria as a function of mitochondrial transmembrane potential ($\Delta\psi_m$) (data not shown). Altogether, these results demonstrate that lactate increased the bioenergetics of human osteoclasts, since it can be used as metabolic fuel by human osteoclasts.

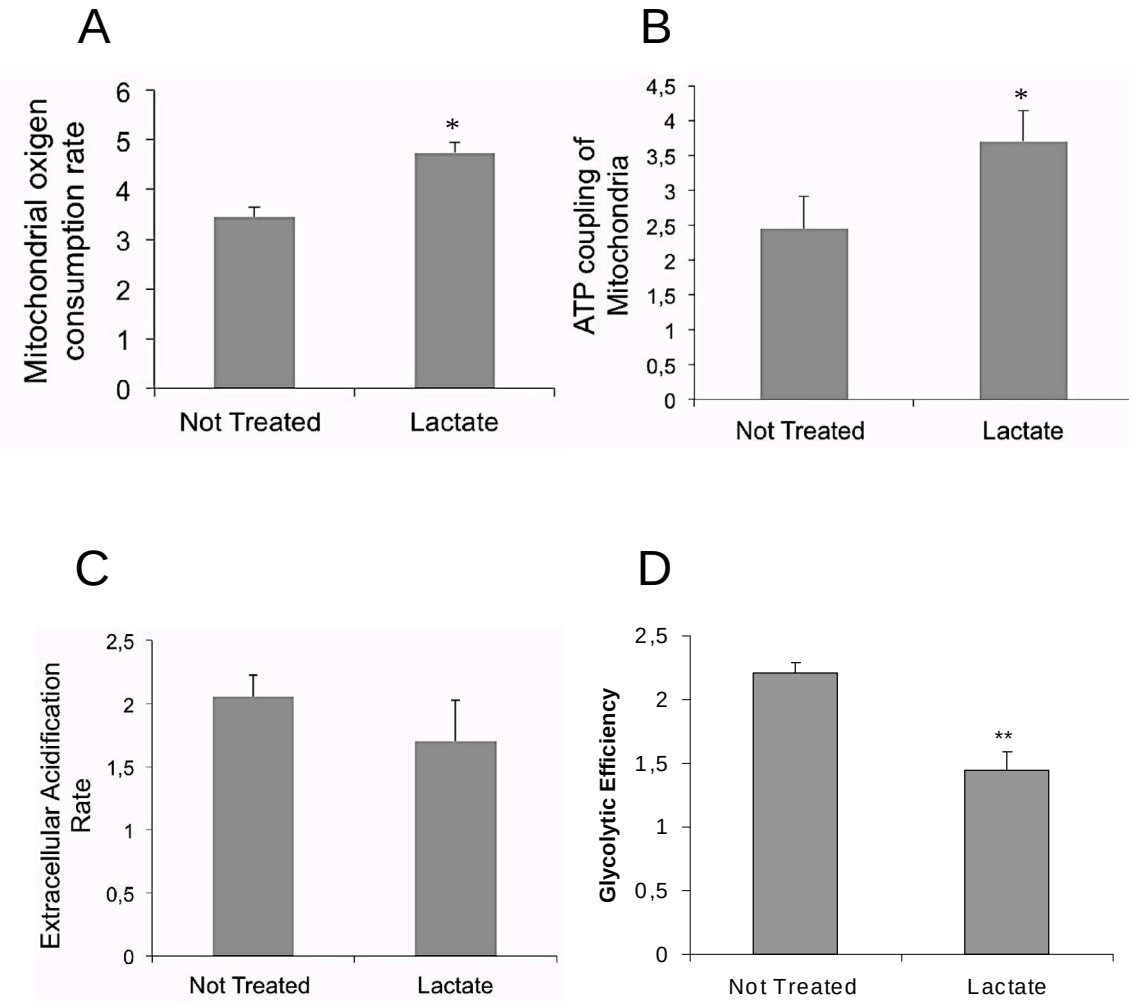

Figure 4.10. Lactate is an oxidative fuel for mature osteoclasts. Osteoclasts were treated

for 7 days with 10 mM sodium lactate in presence of 25 mM glucose. Their metabolic response was quantified using Seahorse XF96 bioanalyzer (A, B, C), and CMA600 enzymatic analyzer (D). *p<0.05, **p<0.01, n=3.

Section 3: Identification and validation of housekeeping genes for gene expression analyses of cancer stem cells

The metastatic microenvironment is composed of several types of cells, including CSC, a minority subset of tumor-initiating cells involved in metastasis formation and relapse. Here, I analysed the most stable housekeeping genes (HKG) for the normalization of qRT-PCR data direct to compare CSC and native tumor cells.

4.3.1 RNA quality control and characterization of CSC

Sphere cultures were established from commercially available cell lines from 3 different sarcoma and 2 carcinoma histotypes (MG-63 for OS, RD for RS, A-673 for ES, MDA-MB-23 for BC, and ACHN for RC), and from a fresh ES biopsy (ES4540).

With the exception of cscMG-63, cscMDA-MB-231, and cscACHN, the stemness-like features for all the CSC cultures included in this study were previously characterized [92,93]. I confirmed the ability of these CSC cell lines to growth as floating aggregates, and the mRNA expression for KLF4, c-Myc, Nanog, and OCT3/4 stemness markers (Fig. 4.11) [151]. The stemness genes were normalised by ACTB, one of the most commonly used HKG.

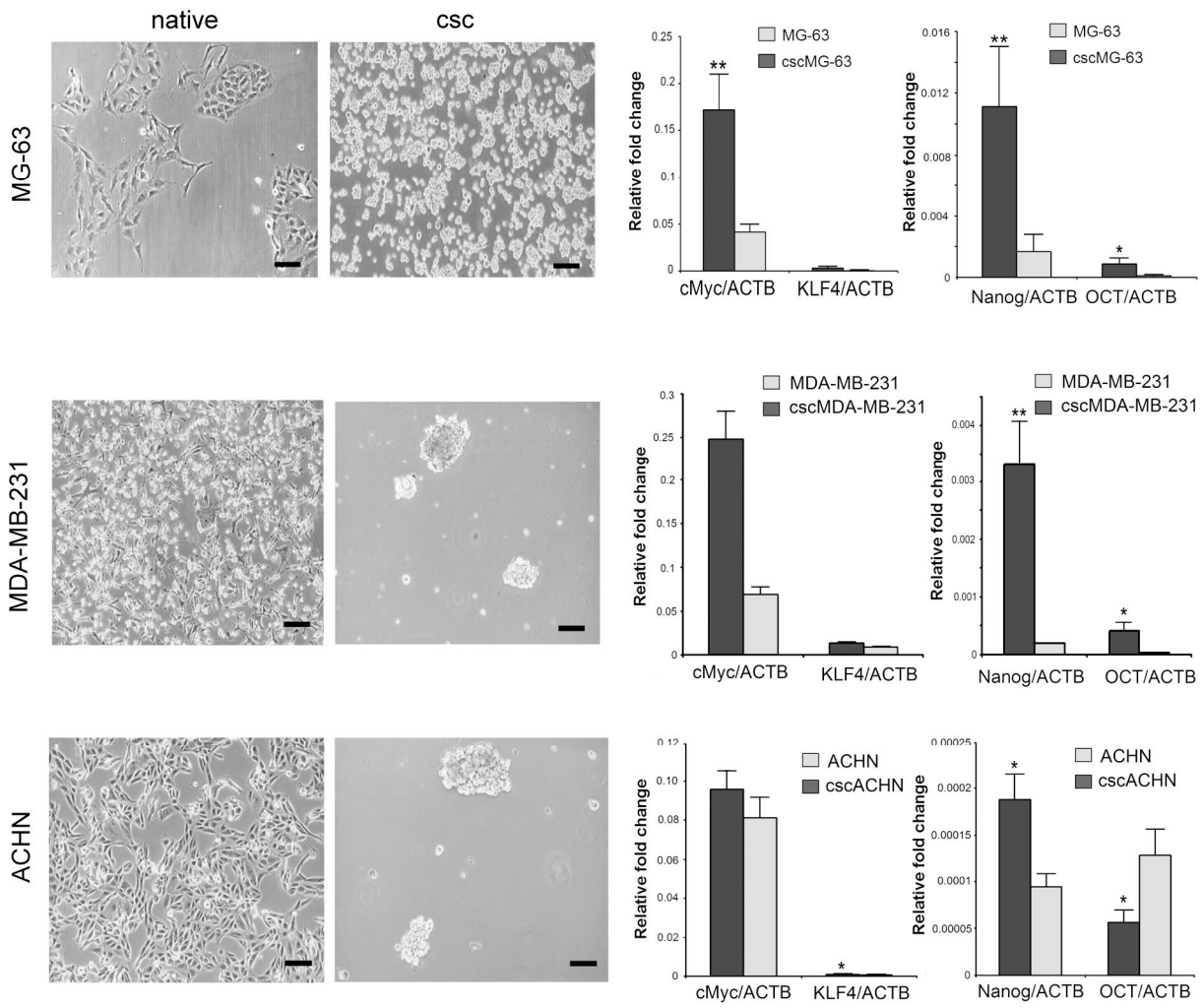

Figure 4.11. Characterization of spheres obtained from MG-63, MDA-MB-231 and ACHN. Representative images of adherent native cells and CSC floating spheres observed by inverted optical microscope for the different cell lines (scale bar 100 µm, left panel), and gene expression of stem cell markers by qRT-PCR (right panel). Normalization to ACTB. For cscMG-63, c-Myc **p=0.0019, KLF4 p=ns, Nanog **p=0.0010, OCT3/4 *p=0.0265. For cscMDA-MB-231, c-Myc **p=0.0011, KLF4 *p=0.0130, Nanog **p=0.0011, OCT3/4 *p=0.0325. For cscACHN, c-Myc p=ns, KLF4 *p=0.0130, Nanog *p=0.0130. For adherent ACHN, OCT3/4 *p=0.0130. n=12. (Reproduced from Lemma S. et al, 2016. PLoS ONE 11(2): e0149481.)

4.3.2 Expression profile of the candidate HKG genes

Fifteen candidate reference genes (Table 3.1) were selected through the analysis of literature survey on studies on normal stem cells and tumor cells with qRT-PCR analysis. We selected those genes that belong to different functional classes or pathways in order to reduce the probability to include in the analysis co-regulated genes. The transcript profiling of the selected genes was preliminary analysed by Illumina Genome Analyzer sequencing. The deep sequencing analysis showed that the putative reference genes were stably expressed, with the exception of G6PD (Table 4.1, Figure 4.12A).

Table 4.1. Transcriptome data from deep sequencing analysis of CSC and native cells of osteosarcoma

Gene	Ensembl ID	Entrez ID	cscMG-63	MG-63	cscHOS	HOS	cscSAOS-2	SAOS-2
ACTB	ENSG00000075624	60	13.565	13.881	13.906	14.208	13.946	14.120
B2M	ENSG00000166710	567	13.117	13.172	12.706	12.564	12.788	13.071
G6PD	ENSG00000160211	2539	10.290	8.851	11.059	10.190	11.559	10.925
GAPDH	ENSG00000111640	2597	13.385	13.511	13.159	13.001	13.385	12.827
GUSB	ENSG00000169919	2990	9.778	9.271	10.630	9.549	11.996	10.151
HMBS	ENSG00000149397	3145	10.035	9.041	10.511	10.912	9.905	9.744
HPRT1	ENSG00000165704	3251	9.304	9.509	10.125	10.475	10.190	10.093
PGK1	ENSG00000102144	5230	12.137	12.440	12.159	12.320	12.895	12.663
PPIA	ENSG00	5478	10.804	11.126	11.472	11.950	10.268	10.620

	0001962 62							
RPL13a	ENSG00 0001425 41	23521	11.081	11.589	11.315	11.732	11.273	11.297
SDHA	ENSG00 0000735 78	6389	11.096	10.548	11.476	11.326	11.813	11.232
TBP	ENSG00 00011259 2	6908	9.238	8.985	8.922	9.017	9.285	9.113
TUBB	ENSG00 0001962 30	203068	13.866	14.479	14.251	14.378	14.059	14.590
YWHAZ	ENSG00 0001649 24	7534	12.379	13.023	11.812	12.737	12.437	12.641

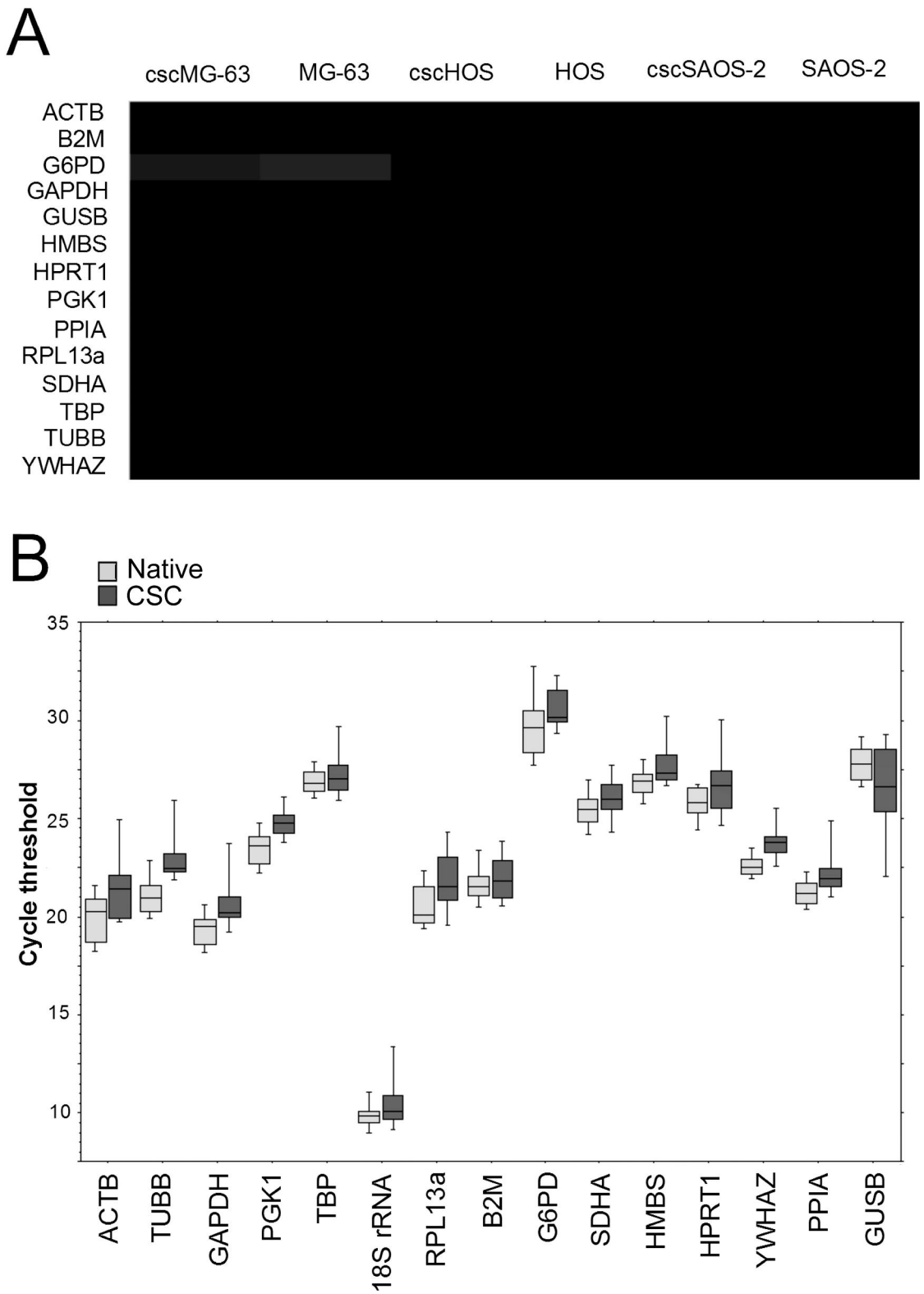

Figure 4.12. Transcription profiling of the selected reference genes. (A) Heat map showing the relative expression of the selected genes in native cells and CSC from MG-63, HOS, and SAOS-2. (B). Transcriptional profile of Cycle threshold (Ct) values of candidate

HKG genes in CSC and native cell lines. Boxes represent lower and upper quartiles of cycle threshold range with the median indicated, vertical bars represent the 10^{th} and 90^{th} percentiles. In both CSC and adherent cell lines, 18S rRNA was the most highly expressed gene (lower Ct value), whereas G6PD was the least expressed gene (highest Ct value). (Reproduced from Lemma S. et al, 2016. PLoS ONE 11(2): e0149481.)

We used only MG-63 as representative of the OS histotype for the following qRT-PCR analysis to confirm the data obtained by deep sequencing. To compare different mRNA transcription levels we used the threshold cycles (Ct) values. Ct value is the intersection between an amplification curve and a threshold line, and is inversely correlated with the amount of target gene present in the PCR reaction [152]. The 15 candidate reference genes exhibited a broad range of expression level. The distribution of median Ct values and percentile for each gene is shown in the blox plot of Figure 4.11B. Reference genes were less expressed in CSC compared to native cells (Table 4.2). By performing the paired Wilcoxon signed-rank test for each gene to evaluate the difference between CSC and native cells obtained from the same cells of origin, we found a significant difference in HKG expression between CSC and native cells for around half of the HKG examined (Table 4.2).

Table 4.2. Ct values of candidate HKG genes in CSC and native cell lines

Gene	**Ct values CSC** [mean ± SD]	**Ct values native cell lines** [mean ± SD]	**qCt values CSC and native cells** [mean ± SDpooled]	**P value**
18S rRNA	10.51 ± 1.53	9.89 ± 0.84	0.62 ± 0.24	N.s.
ACTB	21.58 ± 1.98	19.96 ± 1.42	1.62 ± 0.64	0.0277
B2M	21.95 ± 1.22	21.63 ± 1.13	0.32 ± 0.20	N.s.
G6PD	30.61 ± 1.14	29.82 ± 2.13	0.79 ± 0.61	N.s.
GAPDH	20.72 ± 1.54	19.43 ± 1.01	1.29 ± 0.46	0.0277
GUSB	28.66 ± 2.16	27.81 ± 1.04	0.85 ± 0.34	N.s.
HMBS	27.82 ± 1.30	26.85 ± 0.87	0.97 ± 0.34	N.s.

HPRT1	26.82 ± 1.88	25.84 ± 1.01	0.98 ± 0.37	0.0277
PGK1	24.80 ± 0.81	23.43 ± 0.98	1.37 ± 0.48	0.0277
PPIA	22.27 ± 1.36	21.24 ± 0.77	1.03 ± 0.35	0.0464
RPL13a	21.79 ± 1.64	20.51 ± 1.19	1.28 ± 0.49	0.0464
SDHA	26.01 ± 1.17	25.58 ± 1.09	0.44 ± 0.22	N.s.
TBP	27.32 ± 1.28	26.94 ± 0.89	0.37 ± 0.17	N.s.
TUBB	23.00 ± 1.66	21.07 ± 1.07	1.93 ± 0.65	0.0277
YWHAZ	23.83 ± 1.07	22.60 ± 0.77	1.23 ± 0.40	0.0277

N.s. not significant

4.3.3 Determination of housekeeping gene expression stability

HKG expression stability was evaluated by using NormFinder VBA applet, the GeNorm software, and by calculating and comparing the coefficient of variation (CV) in three different groups: in (1) CSC or (2) native cells, with the aim to identify the most stable genes within a specific cell subtypes, and (3) in the pooled CSC and native cells, with the aim to identify the most stable genes to be considered as reference genes for the comparison of gene expression between CSC and native cells.

The stability values for NormFinder and M values for GeNorm are parameters of stability that are inversely correlated to the expression stability of the HKG. All the 15 candidate reference genes had a M value lower than the threshold value of 1.5 (Table 4.3), which indicated that all can be considered as acceptable in terms of stability [147].

1) The most stable HKG in CSC. Using the NormFinder VBA Applet, the 3 most stable HKG resulted GAPDH, PGK1 and HMBS (from the first to the third stable), whereas the less stable were RPL13a, B2M and GUSB. Using GeNorm software, we identified YWHAZ, GAPDH and TBP as the most stable HKG, whereas the less stable genes were ACTB, GUSB and B2M. CV method also underlined that the use of ACTB should be avoided, whereas, like for GeNorm and NormFinder analyses, the use of PGK1 and YWHAZ is recommended. The

minimal number of reference genes required for normalization was determined by GeNorm calculation of pairwise variation (variation coefficient, V) between a given number of genes and the inclusion of an additional gene, and the optimal number of reference gene was calculated as 3 (V3/4 0.114, Fig. 4.13A). In conclusion, for the gene expression analyses of mRNA isolated from CSC, the optimal normalization factor should be calculated as the geometric mean of the reference targets YWHAZ, GAPDH and PGK1.

2) The most stable HKG in native adherent cells. NormFinder analysis revealed that 18S rRNA, TBP, and PPIA were the three best HKG, whereas RPL13a, G6PD, and ACTB were worse in expression stability. Similarly, GeNorm identified PPIA and 18S rRNA as the two most stable HKG, followed by GAPDH, whereas the less stable genes were G6PD, RPL13a, and ACTB. The CV method suggested HMBS, TBP and YWHAZ as the three most stable genes. The GeNorm calculation of the variation coefficient V suggested that the optimal number of reference genes was 2 (V2/3 0.146; Fig 4.13B). In conclusion, for the native cell the optimal normalization factor should be calculated as the geometric mean of PPIA and TBP.

Table 4.4. Ranking of the stability of the expression of candidate reference genes by NormFinder, geNorm, and CV analyses

		NormFinder		**GeNorm**		**Coefficient of Variation (CV)**	
Group of cells	**Gene**	**Stability value**	**Rank**	**M value**	**Rank**	**CV**	**Rank**
CSC	GAPDH	0.059	1	0.500	2	0.074	11
	PGK1	0.077	2	0.706	8	0.033	1
	HMBS	0.095	3	0.627	7	0.047	5
	YWHAZ	0.101	4	0.516	3	0.045	3
	PPIA	0.102	5	0.528	4	0.061	8
	G6PD	0.104	6	0.761	9	0.037	2
	TUBB	0.119	7	0.611	6	0.072	10

	ACTB	0.138	8	1.095	14	0.092	14
	HPRT1	0.149	9	0.921	12	0.070	9
	SDHA	0.151	10	0.799	10	0.045	4
	B2M	0.153	11	1.179	15	0.055	7
	TBP	0.160	12	0.456	1	0.047	6
	RPL13a	0.162	13	0.850	11	0.075	13
	18S rRNA	0.178	14	0.583	5	0.146	15
	GUSB	0.282	15	1.022	13	0.075	12
Native cells	18S rRNA	0.154	1	0.290	1	0.085	15
	TBP	0.158	2	0.498	4	0.033	2
	PPIA	0.159	3	0.296	2	0.036	4
	SDHA	0.168	4	0.653	7	0.043	8
	GAPDH	0.183	5	0.345	3	0.052	10
	B2M	0.187	6	0.689	8	0.052	11
	HMBS	0.190	7	0.786	11	0.032	1
	HPRT1	0.191	8	0.729	9	0.039	6
	YWHAZ	0.199	9	0.554	5	0.034	3
	TUBB	0.201	10	0.596	6	0.051	9
	GUSB	0.207	11	0.762	10	0.037	5
	PGK1	0.219	12	0.809	12	0.042	7
	RPL13a	0.226	13	0.961	14	0.058	12
	G6PD	0.229	14	1.092	15	0.071	14
	ACTB	0.257	15	0.888	13	0.071	13
CSC and native cells (pooled)	GAPDH	0.124	1	0.484	3	0.086	12
	PPIA	0.134	2	0.437	1	0.066	8
	HMBS	0.141	3	0.689	6	0.051	4
	TBP	0.149	4	0.624	5	0.046	1
	PGK1	0.153	5	0.786	8	0.052	5
	YWHAZ	0.161	6	0.588	4	0.055	6
	G6PD	0.165	7	1.167	15	0.067	10
	18S rRNA	0.168	8	0.470	2	0.143	15
	TUBB	0.168	9	0.735	7	0.091	13
	SDHA	0.172	10	0.821	9	0.050	3
	HPRT1	0.173	11	0.858	10	0.066	9
	B2M	0.182	12	1.037	13	0.050	2
	ACTB	0.192	13	1.104	14	0.103	14
	RPL13a	0.198	14	0.979	12	0.074	11
	GUSB	0.238	15	0.918	11	0.066	7

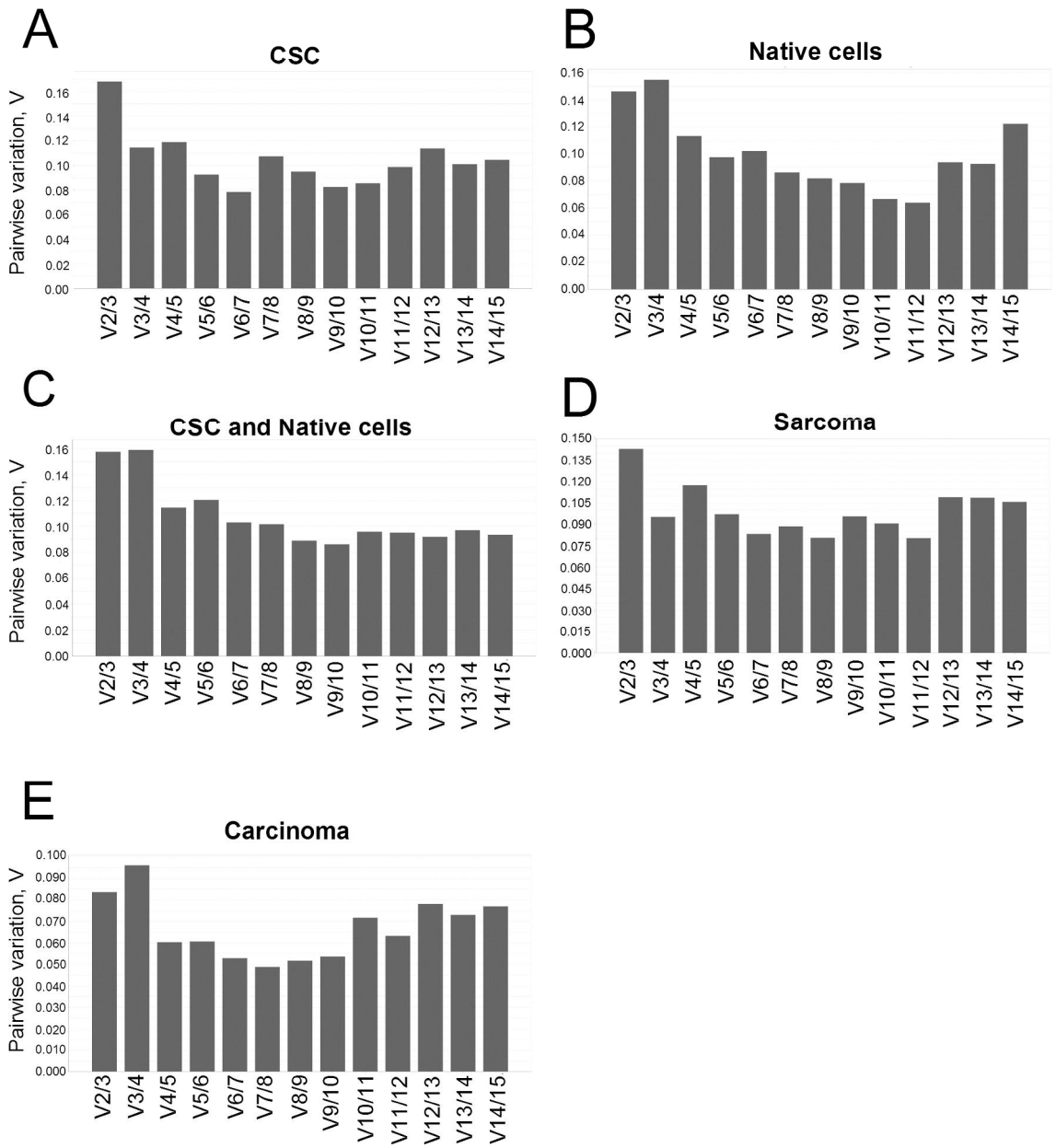

Fig 4.13. GeNorm evaluation of the minimal number of genes and validation of the identified top-ranked HKG genes for qRT-PCR normalization. The minimal number of genes required for data normalization was evaluated by pairwise variation (Vn/n +1) in (A) CSC, (B) native cells, (C) in the CSC and native cell lines from all tumors, (D) from sarcoma and (C) from carcinomas. A variation coefficient (V) below 0.15 indicates the optimal number of genes required for data normalization. (Reproduced from Lemma S. et al, 2016. PLoS ONE 11(2): e0149481.)

3) Finally we performed the analysis of CSC and native pooled cells in all

tumors (A), in sarcoma (B) and carcinoma (C).

(3A) In CSC and native cells from all tumors, NormFinder identified GAPDH, TBP, and PPIA as the three most stable HKG, whereas ACTB, RPL13a and GUSB were the less stable. PPIA and GAPDH were also confirmed by GeNorm analysis, along with 18S rRNA. Again, ACTB was the last gene in stability for the GeNorm analysis, along with B2M and G6PD. The CV evaluation suggested TBP, B2M, and SDHA (Table 4.3). GeNorm recommended the use of 4 HKG for accurate gene expression analysis (V4/5 < 0.15; Fig. 4.13C). Consequently, the normalization factor should be calculated as the geometric mean of TBP, PPIA, HMBS, and YWHAZ or GAPDH.

(3B) In CSC and native cells from sarcoma, the NormFinder software identified GAPDH, YWHAZ and 18S rRNA as the most stable genes. GAPDH and YWHAZ were identified as the best HKG also by the GeNorm analysis. The CV method showed that HMBS, TBP, and SDHA had the best rank position (Table 4.4). The optimal number of reference targets is 2 (V2/3 0.143, Fig. 4.13D). In conclusion, the optimal normalization factor can be calculated as the geometric mean of YWHAZ and GAPDH.

(3C) The analysis of HKG stability in carcinoma revealed that PPIA, HMBS and RPL13a were the most stable HKG for NormFinder. GeNorm also confirmed PPIA and RPL13a as most stable targets by GeNorm, followed by 18S rRNA, whereas the CV method suggested B2M, TBP and G6PD (Table 4.4). The GeNorm calculation of the coefficient V suggested that 2 HKG are sufficient for normalization (V2/3 0.084, Fig. 4.13E). In conclusion, the optimal normalization factor in this case should be calculated as the geometric mean of two of the following genes, PPIA, HMBS or RPL13a.

Table 4.4 Ranking of the stability of the expression of candidate reference genes by NormFinder, geNorm, and CV analyses in CSC and native cells from carcinoma and sarcoma tumors

CSC and native cells (pooled)	Gene	NormFinder		GeNorm		Coefficient of Variation (CV)	
		Stability value	Rank	M value	Rank	CV	Rank
Sarcoma	GAPDH	0.299	1	0.386	1	0.049	9
	YWHAZ	0.346	2	0.434	3	0.036	4
	18S rRNA	0.349	3	0.573	6	0.078	15
	PPIA	0.368	4	0.446	4	0.036	5
	TUBB	0.478	5	0.420	2	0.049	10
	TBP	0.489	6	0.607	7	0.033	2
	SDHA	0.489	7	0.525	5	0.035	3
	PGK1	0.503	8	0.656	8	0.037	6
	HMBS	0.562	9	0.697	9	0.031	1
	HPRT1	0.722	10	0.770	10	0.045	8
	GUSB	0.754	11	0.880	12	0.043	7
	ACTB	0.771	12	1.160	15	0.077	14
	B2M	0.826	13	0.834	11	0.059	11
	RPL13a	0.894	14	0.978	13	0.073	13
	G6PD	0.907	15	1.074	14	0.059	12
Carcinoma	PPIA	0.055	1	0.150	1	0.069	9
	HMBS	0.072	2	0.453	10	0.060	5
	RPL13a	0.088	3	0.193	3	0.075	11
	ACTB	0.091	4	0.390	8	0.092	13
	HPRT1	0.093	5	0.368	7	0.073	10
	18S rRNA	0.093	6	0.164	2	0.144	15
	TBP	0.094	7	0.417	9	0.053	2
	GAPDH	0.103	8	0.298	4	0.088	12
	GUSB	0.104	9	0.315	5	0.066	7
	G6PD	0.140	10	0.521	11	0.054	3
	B2M	0.140	11	0.785	15	0.036	1
	YWHAZ	0.160	12	0.341	6	0.067	8
	TUBB	0.160	13	0.713	14	0.103	14
	PGK1	0.182	14	0.647	13	0.064	6
	SDHA	0.219	15	0.572	12	0.059	4

4.3.4 Validation of the identified HKG in the CSC model

In gene expression evaluation, the use of suboptimal HKG can generate

erroneous results or can hide a difference in gene expression. This is particularly important for genes that slightly change between two populations of cells, such as CSC and native cells.

We analyzed the expression of the stemness genes c-Myc, KLF4, Nanog, and OCT3/4 that were previously normalized to ACTB (Fig. 4.11), with the identified top-ranking HKG for CSC and native cells, in sarcoma and carcinoma, respectively (GAPDH and YWHAZ for sarcoma, and PPIA and HMBS for carcinoma). Some of the stem-related genes considered showed an improved robustness of statistical analysis performed with the normalization with the most stable HKG, in respect with ACTB (Fig. 4.14).

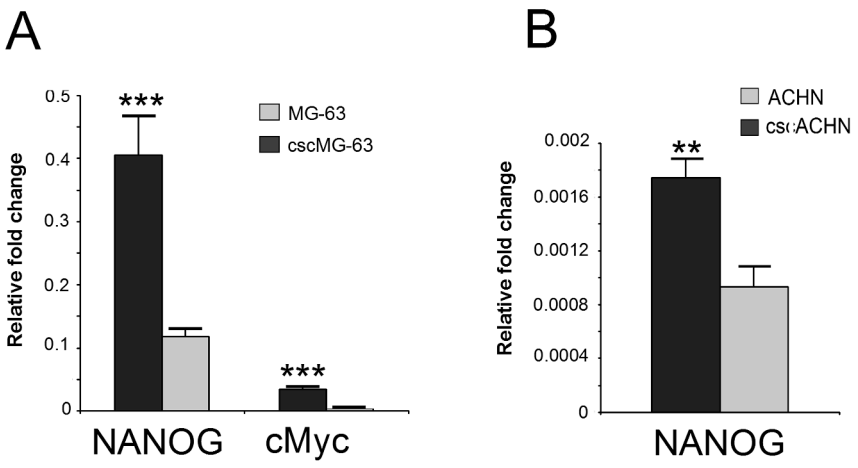

Fig 4.14. Validation of the identified housekeeping genes. The effect of gene expression normalization with optimal HKG was investigated on CSC and native cells from MG-63 and ACHN. (A) For the osteosarcoma cell line, the expression of the stem cell markers Nanog and cMyc were evaluated and normalized to the geometric mean of GAPDH and YWHAZ. ***p=0.0007 for Nanog, ***p=0.0003 for c-Myc. (B) For the ranal carcinoma cell line, the expression of Nanog and cMyc was normalized to the geometric mean of PPIA and HMBS. **p=0.0043 for Nanog. n=6. (Reproduced from Lemma S. et al, 2016. PLoS ONE 11(2): e0149481.)

5. DISCUSSION

In physiological condition, bone homeostasis is maintained by a delicate metabolic equilibrium in bone-relating cells [3]. Osteoclast and osteoblast functions must be tightly regulated to maintain homeostasis. Pathological increases in osteoclast activity induce trabecular bone erosion that result in various diseases, including osteolytic metastases [153]. The development of lytic bone metastasis relies on an exquisite interplay between tumor cells and the machinery orchestrating bone remodeling. Cytokines and hormones produced by the primary tumor are known activators of osteoclastogenesis and osteoclast-mediated bone resorption [17,19,154]; however their therapeutic inactivation is only partially effective, possibly due to the inability of the treatments to interfere with the metabolic pathways that regulate the behavior and the cross-talk between metastatic cells and osteoclasts. In this study, we focused on the metabolic adaptation that occurs in the metastatic microenvironment.

First, we focused on the basal metabolism of human osteoclast, demonstrating that osteoclasts mainly rely on oxidative metabolism for differentiation. Indications about the high metabolic activity of osteoclasts are already apparent, including the presence of a large ATP pool needed for serial stages of osteoclastogenesis and for the fusion of mononuclear precursors to form multinucleated osteoclasts [33]. We analyzed osteoclast metabolism by using primary cell culture of human osteoclasts from PBMC. As proof-of-principle that mature osteoclasts are mitochondria-rich cells [33], we carried out a series of experiments to elucidate the role of mitochondria in osteoclast differentiation. We confirmed that human osteoclasts present increased mitochondria mass and abundant mitochondria, increased in size and rich of cristae, especially if compared with their monocyte precursors. The overall morphology of the

mitochondrial network of mature osteoclasts displayed a complex reticular pattern. Mitochondrial networks spread throughout the cells, from the perinuclear region to the peripheral basal domain. The formation of cluster of mitochondria around the nuclei may be important to efficiently fulfill to biosynthetic functions, whereas the complex reticulum in the basal domain may be important for generating ATP in the peripheral regions of the cell. Considering that mitochondrial biogenesis in associated with an increase expression OxPhos enzymes [35], that cristal membranes are the principal sites of OxPhos [155], and that mitochondrial networks are important for generating ATP in all part of the cell [156], we verified if mitochondrial metabolism is the main bioenergetics driving energy production in mature osteoclasts. Consistently, we found that osteoclasts present high levels of mitochondrial OCR, and low glycolytic efficiency. In control cells, we found a glycolytic efficiency close to 2, which occurs when all the glucose consumed by a cell is converted to lactate, bypassing other metabolic pathways that could utilize glucose or its metabolites. In line with these results, we demonstrated that osteoclasts present increased expression of the complexes of respiratory chain, and high intracellular ATP content, proving that osteoclasts rely on oxidative metabolism for energy production to support the biosynthesis of components demanded for differentiation. Notably, despite results obtained with primary cell cultures of human osteoclasts are usually characterized by a huge variability, we found considerable reproducibility, thereby strongly supporting our conclusions.

Based on our observations, we conclude that osteoclasts are in a high energetic-state sustained by mitochondrial metabolism that might support all the high energy-consuming functions, including bone resorption. Accordingly, we investigated the metabolic pathway underlying osteoclast activity by using glucose or galactose as energy sources. To gain insights into the metabolic

pathway that fuels osteoclast activity, we adjusted media composition with different metabolites, like glucose or galactose as energy sources [149]. The oxidation of galactose to pyruvate through glycolysis yields no net production of ATP, inducing cells to rely on OxPhos to produce energy [157]. We found that when mature osteoclast were cultured with glucose or galactose, they preferentially resorbed type I collagen in presence of glucose, proving that glucose is an essential carbon sources for the acquisition of the resorption activities. Consistently, the combination of galactose and complex I inhibitor rotenone not impaired osteoclast activity, whereas collagen degradation was induced. The regulatory effect of glucose on osteoclast activity is consistent with a previous report showing that glucose regulates the bone resorption of chicken osteoclast at physiological concentration [158]. Other study demonstrates that glucose initiates a series of signaling events that dynamically activates the expression of V-ATPase to stimulate resorption [159]. V-ATPase interact with the glycolytic enzymes phosphofructokinase-1 though the A-subunit [160], and with aldolase though the E-subunit [161], suggesting a direct coupling between the ATP-generating glycolytic enzymes and the ATP-hydrolyzing proton pumps. Proton pumps and ion transporters works hard to transport protons in the cytoplasm of bone resorbing osteoclasts, which then are conveyed into acidic vesicles and released into the extracellular compartment of the resorption lacuna [45,47]. Protons secreted into the resorption lacuna allow the dissolution of hydroxyapatite crystals, and generate the acid environment necessary for the digestion of organic bone matrix by acid proteases [3]. Considering that two protons and two ATP are generated for every molecule of glucose that convey in the glycolytic pathway, it is reasonable to imagine that many proton pumps and glycolytic enzymes can assembly to the ruffled border to compartmentalize ATP and protons generation at functionally-distinct membrane compartments. In

osteoclast, the ruffled border present distinct sub-domains for secretion of acidic vesicle [162], where probably glycolytic enzymes provide ATP to proton pumps that actively convey protons into the resorption lacunae. In a more complete visualization of metabolic state of osteoclast during resorption, we presume that mitochondria networks provide energy in all part of the cell, thereby supporting osteoclast survival, whereas the direct coupling between glycolysis and proton pumps allow a more efficient resorption activity in distinct subdomains of the ruffled border. We expect that osteoclast relies on a spatial and temporal compartmentalization of metabolism to support specific cellular functions in particular cellular subdomains [163]. As previously demonstrated for angiogenic endothelial cells, glycolytic enzymes compartmentalize in lamellipodia and filopodia to allow rapid generation of ATP during the high-energy consuming processes of cell motility [164]. With a similar mechanism, during the energy-consuming process of bone resorption, osteoclast arrange the cytoskeleton to migrate on bone, and to insert the V-ATPases into the ruffled membrane [165], and it is likely that this rearrangement of microtubule and membrane transporter allow the compartmentalization of protons to the front of migration and resorption. Additional studies are urgently needed to highlight the role of metabolic compartmentalization in the regulation of specific cellular function of osteoclasts.

Then, we focused on the effect of the high-energy metabolite lactate produced by highly glycolytic tumor cells on osteoclast metabolism. Current knowledge suggests that lactate, rather than a mere metabolic waste product, is an effective metabolic fuel for oxidative cells, acting as a paracrine-signaling agent both on tumor and host cells. Previous studies demonstrated that lactate could be up take by tumor-associated stromal cells to supports tumor progression [119,139]. We demonstrated that mature osteoclast relies on oxidative metabolism to support

the energy-associated biosynthetic functions necessary to osteoclast formation. The excess of lactate produced by highly aggressive glycolytic tumor cells that spread to the bone can be taken up from osteoclast in the bone metastatic microenvironment through MCT1 expression on the plasmamembrane. We demonstrated that osteoclast expressed high levels of MCT1, and low levels of MCT4. Notably, the expression of MCT1 increased during osteoclastogenesis, and MCT1 promote the dose-dependent up take of lactate from the extracellular to intracellular compartment of mature osteoclasts. Most importantly, the high MCT1 expression observed in human osteoclast cell culture *in vitro* is consistent with its expression by giant osteoclasts in GCT lesions *in vivo*. GCT is a histologically benign osteolytic tumor characterized by prominent osteoclast-like giant cells, and mononuclear osteoclast precursors [142,166]. Indeed, these finding demonstrated that MCT1 expression is predominant in osteoclast cells, both *in vitro* and *in vivo*, and that the MCT1 shuttle is actively involved in lactate uptake in mature osteoclasts. Coherently, MDA-MB-231 breast carcinoma cells and MDA-MB-231 bone met cells prone to form bone metastases, expressed high levels of MCT4, that seem to be higher in the cell line prone to form bone metastases, and significantly lower levels of MCT1; both carcinoma cell lines produced and released high levels of lactate (10 mM) in cell supernatant. Also bone marrow derived MSC expressed notable levels of MCT4, and lower levels of MCT1, whereas osteoblast cells express low levels of both transporters. According to the leading hypothesis, we investigated the effect of lactate produced by highly glycolytic tumor cells on oxidative metabolism of osteoclasts. Consistently, we found that lactate acts as a metabolic fuel in mature osteoclasts, promoting the mitochondrial OCR, the ATP coupling of mitochondria, and reducing the glycolytic efficiency, without affecting the ECAR. These results supports our hypothesis of the metabolic

symbiosis of the bone metastatic microenvironment [167], where the highly glycolysis-dependent breast carcinoma cells release high concentration of lactate through MCT4 in the extracellular space, and osteoclasts take up lactate through the MCT1 shuttle (Fig. 5.1). Once entered into the cytoplasm, lactate fuels the TCA cycle that supports ATP production and the oxidative metabolism of osteoclasts. Similarly, stromal cells exposed to oxidative stress in the BM tumor microenvironment can switch to a more glycolytic metabolism, thereby releasing high amounts of lactate, as well [123]. As demonstrated in other tumor models [168], lactate uptake by tumor-supporting endothelial cells support angiogenesis of the tumor bulk. It is reasonable to postulate that, with a similar mechanisms, lactate exchange between cells of the bone metastatic microenvironment could act both as a signaling molecule to support tumor aggressiveness, and as a metabolic intermediate that fuels the basal metabolism of osteoclasts to further increase oxidative respiration and ATP production.

Taken together, these data strongly support our hypothesis that in physiological conditions OxPhos per se is crucial to sustain osteoclastogenesis and mature osteoclast survival, whereas a glycolytic switch drive the resorption activity of human osteoclasts. The coordination between these metabolic pathways sustains the perfect balance from mature osteoclast formation to the acquisition of bone resorption ability. However, when metastatic tumor cells spread to the bone, they destroy the balance between bone-resident cells to support tumor cell survival and proliferation in the bone microenvironment. Though the metabolic reprogramming of bone resident cells, tumor cells activate osteoclast, thereby leading to a more aggressive tumor phenotype. Further studies are urgently needed to elucidate the role of extracellular lactate on the metastatic microenvironment.

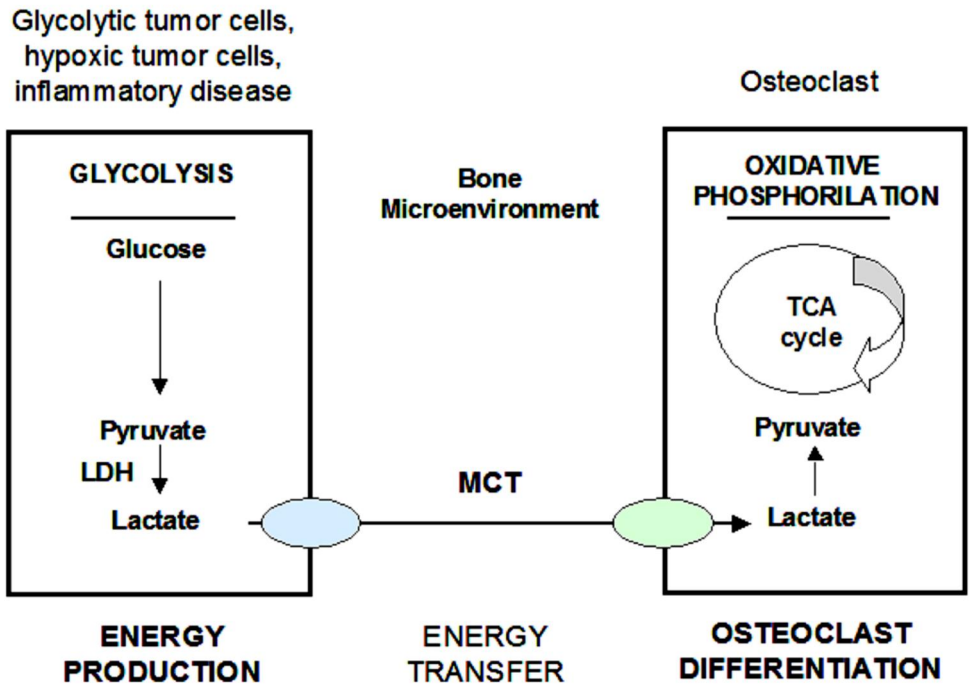

Figure 5.1 Lactate exchange between highly glycolytic cells and osteoclasts in bone microenvironment supports tumor aggressiveness.

In the complex metastatic microenvironment, CSC resides in a niche within the tumor bulk, i.e. a physiologically defined supportive microenvironment, where they interact with other malignant cells leading to a more aggressive tumor phenotype. The evolving concept of CSC has attracted much attention, and characterization of CSC has led the way to novel prospective for anticancer therapies. To study the molecular phenotype of CSC and the underlying cellular mechanism of tumorigenesis, the analysis of gene expression phenotype of native tumor cells and CSC is pivotal. However, despite the recent increasing interest in CSC, an accurate selection of reference genes to a robust normalization of expression data is still missing. We identified and validated the most stable HKG among 15 candidate reference genes for the normalization of qRT-PCR data. We used a panel of CSC and native cell lines from different human sarcoma histotypes, including a tumor primary culture derived from a

human Ewingôs sarcoma biopsy, and from breast and renal carcinoma. Breast carcinoma frequently metastasizes to the bone in the late phases of disease, with devastating consequences for cancer patients. We selected the HKG to be included in this study through a literature survey on the reference genes used for the normalization of qRT-PCR data from normal stem cells [143,169]. Among the normal stem cells, we included MSC [170,171], because they are part of the bone metastatic microenvironment, and represent the most likely candidate cell of origin for osteosarcoma and Ewingôs sarcoma [172,173], and tumor cells [174,175].

As a preliminary analysis of the selected candidate reference genes, we used deep sequencing data, and were able to confirm that the gene expression profile of the selected genes was stable. Then, the expression of the selected genes was validated with qRT-PCR, and we found a broad expression pattern. First of all, we analyzed the homogeneity of expression of the selected HKG in CSC and native cells using the paired Wilcoxon signed-rank test. We found significant difference in gene expression for more than one half of the examined HKG. To evaluate the stability of HKG we first analyzed our data by calculating and comparing the coefficient of variation. Afterwards, we validated the results using NormFider and GeNorm. NormFinder determines the stability value using a model-based approach [59]. GeNorm calculates the expression stability of a gene based on the average pairwise variation among all reference genes [146]. The application of 3 different methods of gene stability evaluation could reduce errors associated with a single software, and could avoid the selection of co-regulated transcripts. We used GeNorm also to determine the minimal number of HKG for accurate normalization. We analyzed the most stable HKG in three groups of data: in CSC, in native cells, and in the CSC and native cells pooled group. By calculating the overall best ranked HKG from the CV, GeNorm and

NormFinder analyses we found that PGK1, YWHAZ, and GAPDH were the most stable HKG for the comparison of CSC expression data, whereas the most stable HKG for native cells were PPIA and TBP. When we considered CSC and native cells with all the tumor types pooled together, we identified TBP, PPIA, HMBS and YWHAZ or GAPDH as HKG that should be used for qRT-PCR normalization. The most stable HKG for the CSC and native cells obtained only from sarcoma were GAPDH and YWHAZ, whereas for carcinoma we identified PPIA, HMBS or RPL13a. Our evaluation of HKG stability also suggested that ACTB and B2M, two of the most commonly used HKG used in qRT-PCR analyses [174-176], but also RPL13a, ranked among the last position in all the considered conditions, suggesting that these HKG could be unsuitable for the normalization of qRT-PCR data. Adversely, in carcinoma, RPL13a ranked between the most stable HKG in CSC and native cells. Therefore, appropriate HKG should be selected in relation to the tumor investigated. Moreover, the analysis of stemness genes KLF4, c-Myc, Nanog, and OCT3/4 to ACTB rather than to the most stable HKG in CSC and native cells, clearly demonstrated that normalization to the suboptimal HKG can lead to a complete loss of information about the stamness capacity of CSC, or can hide difference in gene expression between CSC and native cells. Taken together, our results demonstrate that proper reference genes should be appropriately selected under different experimental conditions. We recommend to use at least two of the suggested HKG to normalize qRT-PCR-based gene expression analyses of human CSC and native cells.

6. CONCLUSION

Bone metastases are composed of a combination of tumor-associated stromal cells, osteoblasts, osteoclasts, CSC, and tumor cells, and the metabolic influences between these different cell types promote tumor progression and lesions formation. To investigate the metabolic symbiosis of lytic bone metastases, we first focused our attention on the basal metabolism of human osteoclast, demonstrating that human osteoclast display an oxidative basal metabolism that supports osteoclast differentiation from hematopoietic precursors. A glycolytic switch drives the acquisition of resorption activity of osteoclasts, suggesting that mitochondrial metabolism and glycolysis co-coordinately regulates osteoclastogenesis and the activation of bone resorption. Understanding the metabolic adaptations underling the coordination of bioenergetics in human osteoclast differentiation and function could provide novel opportunities for therapeutic intervention on metabolic bone diseases caused by osteoclastic dysfunction, in particular lytic bone metastasis. Notably, we found that in the bone metastatic microenvironment, lactate derived from highly glycolytic tumor cells fuels the oxidative metabolism of human osteoclast, leading to a more aggressive tumor phenotype, demonstrating that cancer cells and bone-resident cells sustain each other in a metabolic symbiosis aimed to support the metabolic needs of tumor bulk.

The role of CSC in metastatic cancer is still under investigation. Future studies will focus on the dialogue between CSC, osteoclasts and other malignant-associated cells to elucidate the role of the metabolic symbiosis in lytic bone metastasis.

7. REFERENCES

1. Ferlay J, Soerjomataram I, Dikshit R, Eser S, Mathers C, et al. (2015) Cancer incidence and mortality worldwide: sources, methods and major patterns in GLOBOCAN 2012. Int J Cancer 136: E359-386.
2. Plunkett TA, Smith P, Rubens RD (2000) Risk of complications from bone metastases in breast cancer. implications for management. Eur J Cancer 36: 476-482.
3. Teitelbaum SL (2000) Bone resorption by osteoclasts. Science 289: 1504-1508.
4. Zaidi M (2007) Skeletal remodeling in health and disease. Nat Med 13: 791-801.
5. Coleman RE (2006) Clinical features of metastatic bone disease and risk of skeletal morbidity. Clin Cancer Res 12: 6243s-6249s.
6. Kakonen SM, Mundy GR (2003) Mechanisms of osteolytic bone metastases in breast carcinoma. Cancer 97: 834-839.
7. Clarke B (2008) Normal bone anatomy and physiology. Clin J Am Soc Nephrol 3 Suppl 3: S131-139.
8. Harada S, Rodan GA (2003) Control of osteoblast function and regulation of bone mass. Nature 423: 349-355.
9. Neer RM, Arnaud CD, Zanchetta JR, Prince R, Gaich GA, et al. (2001) Effect of parathyroid hormone (1-34) on fractures and bone mineral density in postmenopausal women with osteoporosis. N Engl J Med 344: 1434-1441.
10. Massey HM, Flanagan AM (1999) Human osteoclasts derive from CD14-positive monocytes. Br J Haematol 106: 167-170.
11. Boyle WJ, Simonet WS, Lacey DL (2003) Osteoclast differentiation and activation. Nature 423: 337-342.
12. Blair JM, Zheng Y, Dunstan CR (2007) RANK ligand. Int J Biochem Cell Biol 39: 1077-1081.
13. Novack DV (2011) Role of NF-kappaB in the skeleton. Cell Res 21: 169-182.
14. Sun SC (2012) The noncanonical NF-kappaB pathway. Immunol Rev 246: 125-140.
15. Theoleyre S, Wittrant Y, Tat SK, Fortun Y, Redini F, et al. (2004) The molecular triad OPG/RANK/RANKL: involvement in the orchestration of pathophysiological bone remodeling. Cytokine Growth Factor Rev 15: 457-475.
16. Cenni E, Perut F, Granchi D, Amato I, Avnet S, et al. (2006) Primitive and

bone metastatic renal carcinoma cells promote osteoclastogenesis through endothelial cells. Anticancer Res 26: 3065-3069.
17. Granchi D, Amato I, Battistelli L, Avnet S, Capaccioli S, et al. (2004) In vitro blockade of receptor activator of nuclear factor-kappaB ligand prevents osteoclastogenesis induced by neuroblastoma cells. Int J Cancer 111: 829-838.
18. Granchi D, Amato I, Battistelli L, Ciapetti G, Pagani S, et al. (2005) Molecular basis of osteoclastogenesis induced by osteoblasts exposed to wear particles. Biomaterials 26: 2371-2379.
19. Avnet S, Salerno M, Quacquaruccio G, Granchi D, Giunti A, et al. (2011) IGF2 derived from SH-SY5Y neuroblastoma cells induces the osteoclastogenesis of human monocytic precursors. Exp Cell Res 317: 2147-2158.
20. Martin TJ, Udagawa N (1998) Hormonal regulation of osteoclast function. Trends Endocrinol Metab 9: 6-12.
21. Broxmeyer HE, Cooper S, Lu L, Miller ME, Langefeld CD, et al. (1990) Enhanced stimulation of human bone marrow macrophage colony formation in vitro by recombinant human macrophage colony-stimulating factor in agarose medium and at low oxygen tension. Blood 76: 323-329.
22. Utting JC, Flanagan AM, Brandao-Burch A, Orriss IR, Arnett TR (2010) Hypoxia stimulates osteoclast formation from human peripheral blood. Cell Biochem Funct 28: 374-380.
23. Knowles HJ, Cleton-Jansen AM, Korsching E, Athanasou NA (2010) Hypoxia-inducible factor regulates osteoclast-mediated bone resorption: role of angiopoietin-like 4. FASEB J 24: 4648-4659.
24. Knowles HJ, Athanasou NA (2009) Acute hypoxia and osteoclast activity: a balance between enhanced resorption and increased apoptosis. J Pathol 218: 256-264.
25. Arnett TR, Gibbons DC, Utting JC, Orriss IR, Hoebertz A, et al. (2003) Hypoxia is a major stimulator of osteoclast formation and bone resorption. J Cell Physiol 196: 2-8.
26. Arnett TR (2010) Acidosis, hypoxia and bone. Arch Biochem Biophys 503: 103-109.
27. Knowles HJ, Athanasou NA (2008) Hypoxia-inducible factor is expressed in giant cell tumour of bone and mediates paracrine effects of hypoxia on monocyte-osteoclast differentiation via induction of VEGF. J Pathol 215: 56-66.
28. Morten KJ, Badder L, Knowles HJ (2013) Differential regulation of HIF-mediated pathways increases mitochondrial metabolism and ATP production in hypoxic osteoclasts. J Pathol 229: 755-764.
29. Indo Y, Takeshita S, Ishii KA, Hoshii T, Aburatani H, et al. (2013) Metabolic

regulation of osteoclast differentiation and function. J Bone Miner Res 28: 2392-2399.
30. Morrison MS, Turin L, King BF, Burnstock G, Arnett TR (1998) ATP is a potent stimulator of the activation and formation of rodent osteoclasts. J Physiol 511 (Pt 2): 495-500.
31. Jin Z, Wei W, Yang M, Du Y, Wan Y (2014) Mitochondrial complex I activity suppresses inflammation and enhances bone resorption by shifting macrophage-osteoclast polarization. Cell Metab 20: 483-498.
32. Baron R, Neff L, Tran Van P, Nefussi JR, Vignery A (1986) Kinetic and cytochemical identification of osteoclast precursors and their differentiation into multinucleated osteoclasts. Am J Pathol 122: 363-378.
33. Miyazaki T, Iwasawa M, Nakashima T, Mori S, Shigemoto K, et al. (2012) Intracellular and extracellular ATP coordinately regulate the inverse correlation between osteoclast survival and bone resorption. J Biol Chem 287: 37808-37823.
34. Czupalla C, Mansukoski H, Pursche T, Krause E, Hoflack B (2005) Comparative study of protein and mRNA expression during osteoclastogenesis. Proteomics 5: 3868-3875.
35. Ishii KA, Fumoto T, Iwai K, Takeshita S, Ito M, et al. (2009) Coordination of PGC-1beta and iron uptake in mitochondrial biogenesis and osteoclast activation. Nat Med 15: 259-266.
36. Wei W, Wang X, Yang M, Smith LC, Dechow PC, et al. (2010) PGC1beta mediates PPARgamma activation of osteoclastogenesis and rosiglitazone-induced bone loss. Cell Metab 11: 503-516.
37. Zhou J, Ye S, Fujiwara T, Manolagas SC, Zhao H (2013) Steap4 plays a critical role in osteoclastogenesis in vitro by regulating cellular iron/reactive oxygen species (ROS) levels and cAMP response element-binding protein (CREB) activation. J Biol Chem 288: 30064-30074.
38. Zeng R, Faccio R, Novack DV (2015) Alternative NF-kappaB Regulates RANKL-Induced Osteoclast Differentiation and Mitochondrial Biogenesis via Independent Mechanisms. J Bone Miner Res 30: 2287-2299.
39. Vaananen K (2005) Mechanism of osteoclast mediated bone resorption--rationale for the design of new therapeutics. Adv Drug Deliv Rev 57: 959-971.
40. Lakkakorpi P, Tuukkanen J, Hentunen T, Jarvelin K, Vaananen K (1989) Organization of osteoclast microfilaments during the attachment to bone surface in vitro. J Bone Miner Res 4: 817-825.
41. Lakkakorpi PT, Vaananen HK (1991) Kinetics of the osteoclast cytoskeleton during the resorption cycle in vitro. J Bone Miner Res 6: 817-826.
42. Marchisio PC, Bergui L, Corbascio GC, Cremona O, D'Urso N, et al. (1988)

Vinculin, talin, and integrins are localized at specific adhesion sites of malignant B lymphocytes. Blood 72: 830-833.
43. Lakkakorpi PT, Horton MA, Helfrich MH, Karhukorpi EK, Vaananen HK (1991) Vitronectin receptor has a role in bone resorption but does not mediate tight sealing zone attachment of osteoclasts to the bone surface. J Cell Biol 115: 1179-1186.
44. Palokangas H, Mulari M, Vaananen HK (1997) Endocytic pathway from the basal plasma membrane to the ruffled border membrane in bone-resorbing osteoclasts. J Cell Sci 110 (Pt 15): 1767-1780.
45. Blair HC, Teitelbaum SL, Ghiselli R, Gluck S (1989) Osteoclastic bone resorption by a polarized vacuolar proton pump. Science 245: 855-857.
46. Qin A, Cheng TS, Pavlos NJ, Lin Z, Dai KR, et al. (2012) V-ATPases in osteoclasts: structure, function and potential inhibitors of bone resorption. Int J Biochem Cell Biol 44: 1422-1435.
47. Rousselle AV, Heymann D (2002) Osteoclastic acidification pathways during bone resorption. Bone 30: 533-540.
48. Francis MJ, Lees RL, Trujillo E, Martin-Vasallo P, Heersche JN, et al. (2002) ATPase pumps in osteoclasts and osteoblasts. Int J Biochem Cell Biol 34: 459-476.
49. Valastyan S, Weinberg RA (2011) Tumor metastasis: molecular insights and evolving paradigms. Cell 147: 275-292.
50. Liotta LA, Kohn E (1990) Cancer invasion and metastases. JAMA 263: 1123-1126.
51. Woodhouse EC, Chuaqui RF, Liotta LA (1997) General mechanisms of metastasis. Cancer 80: 1529-1537.
52. Onuigbo WI (1977) Paradoxical position of vertebral veins in cancer carriage. Med Hypotheses 3: 267-269.
53. Kim YS, Liotta LA, Kohn EC (1993) Cancer invasion and metastasis. Hosp Pract (Off Ed) 28: 92-96.
54. Coleman RE (1997) Skeletal complications of malignancy. Cancer 80: 1588-1594.
55. Paget S (1989) The distribution of secondary growths in cancer of the breast. 1889. Cancer Metastasis Rev 8: 98-101.
56. Ozdemir BC, Hensel J, Secondini C, Wetterwald A, Schwaninger R, et al. (2014) The molecular signature of the stroma response in prostate cancer-induced osteoblastic bone metastasis highlights expansion of hematopoietic and prostate epithelial stem cell niches. PLoS One 9: e114530.
57. Coleman RE (2001) Metastatic bone disease: clinical features, pathophysiology and treatment strategies. Cancer Treat Rev 27: 165-176.
58. Zetter BR (1990) The cellular basis of site-specific tumor metastasis. N Engl

J Med 322: 605-612.
59. Mundy GR (2002) Metastasis to bone: causes, consequences and therapeutic opportunities. Nat Rev Cancer 2: 584-593.
60. Kingsley LA, Fournier PG, Chirgwin JM, Guise TA (2007) Molecular biology of bone metastasis. Mol Cancer Ther 6: 2609-2617.
61. Kozlow W, Guise TA (2005) Breast cancer metastasis to bone: mechanisms of osteolysis and implications for therapy. J Mammary Gland Biol Neoplasia 10: 169-180.
62. Yoneda T, Hiraga T (2005) Crosstalk between cancer cells and bone microenvironment in bone metastasis. Biochem Biophys Res Commun 328: 679-687.
63. Mundy GR, Guise TA (1997) Hypercalcemia of malignancy. Am J Med 103: 134-145.
64. Chambers AF, Groom AC, MacDonald IC (2002) Dissemination and growth of cancer cells in metastatic sites. Nat Rev Cancer 2: 563-572.
65. Weilbaecher KN, Guise TA, McCauley LK (2011) Cancer to bone: a fatal attraction. Nat Rev Cancer 11: 411-425.
66. Park SI, Soki FN, McCauley LK (2011) Roles of bone marrow cells in skeletal metastases: no longer bystanders. Cancer Microenviron 4: 237-246.
67. Fessler E, Dijkgraaf FE, De Sousa EMF, Medema JP (2013) Cancer stem cell dynamics in tumor progression and metastasis: is the microenvironment to blame? Cancer Lett 341: 97-104.
68. Lee KM, Nam K, Oh S, Lim J, Kim RK, et al. (2015) ECM1 regulates tumor metastasis and CSC-like property through stabilization of beta-catenin. Oncogene 34: 6055-6065.
69. Kuo TC, Chen CT, Baron D, Onder TT, Loewer S, et al. (2011) Midbody accumulation through evasion of autophagy contributes to cellular reprogramming and tumorigenicity. Nat Cell Biol 13: 1214-1223.
70. Liu H, Patel MR, Prescher JA, Patsialou A, Qian D, et al. (2010) Cancer stem cells from human breast tumors are involved in spontaneous metastases in orthotopic mouse models. Proc Natl Acad Sci U S A 107: 18115-18120.
71. Medema JP, Vermeulen L (2011) Microenvironmental regulation of stem cells in intestinal homeostasis and cancer. Nature 474: 318-326.
72. Rose AA, Siegel PM (2006) Breast cancer-derived factors facilitate osteolytic bone metastasis. Bull Cancer 93: 931-943.
73. Clines GA, Guise TA (2008) Molecular mechanisms and treatment of bone metastasis. Expert Rev Mol Med 10: e7.
74. Powell GJ, Southby J, Danks JA, Stillwell RG, Hayman JA, et al. (1991) Localization of parathyroid hormone-related protein in breast cancer

metastases: increased incidence in bone compared with other sites. Cancer Res 51: 3059-3061.
75. Guise TA (1997) Parathyroid hormone-related protein and bone metastases. Cancer 80: 1572-1580.
76. Edwards JR, Mundy GR (2011) Advances in osteoclast biology: old findings and new insights from mouse models. Nat Rev Rheumatol 7: 235-243.
77. Feinberg AP, Ohlsson R, Henikoff S (2006) The epigenetic progenitor origin of human cancer. Nat Rev Genet 7: 21-33.
78. Visvader JE, Lindeman GJ (2008) Cancer stem cells in solid tumours: accumulating evidence and unresolved questions. Nat Rev Cancer 8: 755-768.
79. Patrawala L, Calhoun T, Schneider-Broussard R, Li H, Bhatia B, et al. (2006) Highly purified CD44+ prostate cancer cells from xenograft human tumors are enriched in tumorigenic and metastatic progenitor cells. Oncogene 25: 1696-1708.
80. Hermann PC, Huber SL, Herrler T, Aicher A, Ellwart JW, et al. (2007) Distinct populations of cancer stem cells determine tumor growth and metastatic activity in human pancreatic cancer. Cell Stem Cell 1: 313-323.
81. Mueller MT, Hermann PC, Heeschen C (2010) Cancer stem cells as new therapeutic target to prevent tumour progression and metastasis. Front Biosci (Elite Ed) 2: 602-613.
82. Bao S, Wu Q, McLendon RE, Hao Y, Shi Q, et al. (2006) Glioma stem cells promote radioresistance by preferential activation of the DNA damage response. Nature 444: 756-760.
83. Li X, Lewis MT, Huang J, Gutierrez C, Osborne CK, et al. (2008) Intrinsic resistance of tumorigenic breast cancer cells to chemotherapy. J Natl Cancer Inst 100: 672-679.
84. Hambardzumyan D, Becher OJ, Rosenblum MK, Pandolfi PP, Manova-Todorova K, et al. (2008) PI3K pathway regulates survival of cancer stem cells residing in the perivascular niche following radiation in medulloblastoma in vivo. Genes Dev 22: 436-448.
85. Clarke MF, Fuller M (2006) Stem cells and cancer: two faces of eve. Cell 124: 1111-1115.
86. Jordan CT, Guzman ML, Noble M (2006) Cancer stem cells. N Engl J Med 355: 1253-1261.
87. Al-Hajj M, Wicha MS, Benito-Hernandez A, Morrison SJ, Clarke MF (2003) Prospective identification of tumorigenic breast cancer cells. Proc Natl Acad Sci U S A 100: 3983-3988.
88. Lapidot T, Sirard C, Vormoor J, Murdoch B, Hoang T, et al. (1994) A cell initiating human acute myeloid leukaemia after transplantation into SCID mice. Nature 367: 645-648.

89. Bonnet D, Dick JE (1997) Human acute myeloid leukemia is organized as a hierarchy that originates from a primitive hematopoietic cell. Nat Med 3: 730-737.
90. Singh SK, Clarke ID, Terasaki M, Bonn VE, Hawkins C, et al. (2003) Identification of a cancer stem cell in human brain tumors. Cancer Res 63: 5821-5828.
91. Ponti D, Costa A, Zaffaroni N, Pratesi G, Petrangolini G, et al. (2005) Isolation and in vitro propagation of tumorigenic breast cancer cells with stem/progenitor cell properties. Cancer Res 65: 5506-5511.
92. Salerno M, Avnet S, Bonuccelli G, Eramo A, De Maria R, et al. (2013) Sphere-forming cell subsets with cancer stem cell properties in human musculoskeletal sarcomas. Int J Oncol 43: 95-102.
93. Salerno M, Avnet S, Bonuccelli G, Hosogi S, Granchi D, et al. (2014) Impairment of lysosomal activity as a therapeutic modality targeting cancer stem cells of embryonal rhabdomyosarcoma cell line RD. PLoS One 9: e110340.
94. Gibbs CP, Kukekov VG, Reith JD, Tchigrinova O, Suslov ON, et al. (2005) Stem-like cells in bone sarcomas: implications for tumorigenesis. Neoplasia 7: 967-976.
95. Wang L, Park P, Lin CY (2009) Characterization of stem cell attributes in human osteosarcoma cell lines. Cancer Biol Ther 8: 543-552.
96. Suva ML, Riggi N, Janiszewska M, Radovanovic I, Provero P, et al. (2009) EZH2 is essential for glioblastoma cancer stem cell maintenance. Cancer Res 69: 9211-9218.
97. Sette G, Salvati V, Memeo L, Fecchi K, Colarossi C, et al. (2012) EGFR inhibition abrogates leiomyosarcoma cell chemoresistance through inactivation of survival pathways and impairment of CSC potential. PLoS One 7: e46891.
98. Bernards R, Weinberg RA (2002) A progression puzzle. Nature 418: 823.
99. Minn AJ, Gupta GP, Siegel PM, Bos PD, Shu W, et al. (2005) Genes that mediate breast cancer metastasis to lung. Nature 436: 518-524.
100. Minn AJ, Kang Y, Serganova I, Gupta GP, Giri DD, et al. (2005) Distinct organ-specific metastatic potential of individual breast cancer cells and primary tumors. J Clin Invest 115: 44-55.
101. Kang Y (2005) Functional genomic analysis of cancer metastasis: biologic insights and clinical implications. Expert Rev Mol Diagn 5: 385-395.
102. Li F, Tiede B, Massague J, Kang Y (2007) Beyond tumorigenesis: cancer stem cells in metastasis. Cell Res 17: 3-14.
103. Cairns RA, Harris IS, Mak TW (2011) Regulation of cancer cell metabolism. Nat Rev Cancer 11: 85-95.
104. Levine AJ, Puzio-Kuter AM (2010) The control of the metabolic switch in

cancers by oncogenes and tumor suppressor genes. Science 330: 1340-1344.
105. Dewhirst MW (2003) Mechanisms underlying hypoxia development in tumors. Adv Exp Med Biol 510: 51-56.
106. Spencer JA, Ferraro F, Roussakis E, Klein A, Wu J, et al. (2014) Direct measurement of local oxygen concentration in the bone marrow of live animals. Nature 508: 269-273.
107. Marenzana M, Arnett TR (2013) The Key Role of the Blood Supply to Bone. Bone Res 1: 203-215.
108. Dang CV, Semenza GL (1999) Oncogenic alterations of metabolism. Trends Biochem Sci 24: 68-72.
109. Warburg O, Wind F, Negelein E (1927) The Metabolism of Tumors in the Body. J Gen Physiol 8: 519-530.
110. Warburg O (1956) On the origin of cancer cells. Science 123: 309-314.
111. Gatenby RA, Gillies RJ (2004) Why do cancers have high aerobic glycolysis? Nat Rev Cancer 4: 891-899.
112. James PE, Jackson SK, Grinberg OY, Swartz HM (1995) The effects of endotoxin on oxygen consumption of various cell types in vitro: an EPR oximetry study. Free Radic Biol Med 18: 641-647.
113. Bissell MJ, Radisky D (2001) Putting tumours in context. Nat Rev Cancer 1: 46-54.
114. Marx J (2008) Cancer biology. All in the stroma: cancer's Cosa Nostra. Science 320: 38-41.
115. Bergfeld SA, DeClerck YA (2010) Bone marrow-derived mesenchymal stem cells and the tumor microenvironment. Cancer Metastasis Rev 29: 249-261.
116. Bonuccelli G, Tsirigos A, Whitaker-Menezes D, Pavlides S, Pestell RG, et al. (2010) Ketones and lactate "fuel" tumor growth and metastasis: Evidence that epithelial cancer cells use oxidative mitochondrial metabolism. Cell Cycle 9: 3506-3514.
117. Pavlides S, Whitaker-Menezes D, Castello-Cros R, Flomenberg N, Witkiewicz AK, et al. (2009) The reverse Warburg effect: aerobic glycolysis in cancer associated fibroblasts and the tumor stroma. Cell Cycle 8: 3984-4001.
118. Martinez-Outschoorn UE, Balliet RM, Rivadeneira DB, Chiavarina B, Pavlides S, et al. (2010) Oxidative stress in cancer associated fibroblasts drives tumor-stroma co-evolution: A new paradigm for understanding tumor metabolism, the field effect and genomic instability in cancer cells. Cell Cycle 9: 3256-3276.
119. Fiaschi T, Marini A, Giannoni E, Taddei ML, Gandellini P, et al. (2012) Reciprocal metabolic reprogramming through lactate shuttle coordinately

influences tumor-stroma interplay. Cancer Res 72: 5130-5140.
120. Bonuccelli G, Avnet S, Grisendi G, Salerno M, Granchi D, et al. (2014) Role of mesenchymal stem cells in osteosarcoma and metabolic reprogramming of tumor cells. Oncotarget 5: 7575-7588.
121. Curry JM, Tuluc M, Whitaker-Menezes D, Ames JA, Anantharaman A, et al. (2013) Cancer metabolism, stemness and tumor recurrence: MCT1 and MCT4 are functional biomarkers of metabolic symbiosis in head and neck cancer. Cell Cycle 12: 1371-1384.
122. Dhup S, Dadhich RK, Porporato PE, Sonveaux P (2012) Multiple biological activities of lactic acid in cancer: influences on tumor growth, angiogenesis and metastasis. Curr Pharm Des 18: 1319-1330.
123. Sonveaux P, Vegran F, Schroeder T, Wergin MC, Verrax J, et al. (2008) Targeting lactate-fueled respiration selectively kills hypoxic tumor cells in mice. J Clin Invest 118: 3930-3942.
124. Hirschhaeuser F, Sattler UG, Mueller-Klieser W (2011) Lactate: a metabolic key player in cancer. Cancer Res 71: 6921-6925.
125. Walenta S, Salameh A, Lyng H, Evensen JF, Mitze M, et al. (1997) Correlation of high lactate levels in head and neck tumors with incidence of metastasis. Am J Pathol 150: 409-415.
126. Walenta S, Wetterling M, Lehrke M, Schwickert G, Sundfor K, et al. (2000) High lactate levels predict likelihood of metastases, tumor recurrence, and restricted patient survival in human cervical cancers. Cancer Res 60: 916-921.
127. Brizel DM, Schroeder T, Scher RL, Walenta S, Clough RW, et al. (2001) Elevated tumor lactate concentrations predict for an increased risk of metastases in head-and-neck cancer. Int J Radiat Oncol Biol Phys 51: 349-353.
128. Doherty JR, Cleveland JL (2013) Targeting lactate metabolism for cancer therapeutics. J Clin Invest 123: 3685-3692.
129. Vegran F, Boidot R, Michiels C, Sonveaux P, Feron O (2011) Lactate influx through the endothelial cell monocarboxylate transporter MCT1 supports an NF-kappaB/IL-8 pathway that drives tumor angiogenesis. Cancer Res 71: 2550-2560.
130. Hunt TK, Aslam RS, Beckert S, Wagner S, Ghani QP, et al. (2007) Aerobically derived lactate stimulates revascularization and tissue repair via redox mechanisms. Antioxid Redox Signal 9: 1115-1124.
131. Halestrap AP, Wilson MC (2012) The monocarboxylate transporter family--role and regulation. IUBMB Life 64: 109-119.
132. Draoui N, Feron O (2011) Lactate shuttles at a glance: from physiological paradigms to anti-cancer treatments. Dis Model Mech 4: 727-732.
133. Halestrap AP (2013) The SLC16 gene family - structure, role and

regulation in health and disease. Mol Aspects Med 34: 337-349.
134. Wilson MC, Meredith D, Fox JE, Manoharan C, Davies AJ, et al. (2005) Basigin (CD147) is the target for organomercurial inhibition of monocarboxylate transporter isoforms 1 and 4: the ancillary protein for the insensitive MCT2 is EMBIGIN (gp70). J Biol Chem 280: 27213-27221.
135. Kirk P, Wilson MC, Heddle C, Brown MH, Barclay AN, et al. (2000) CD147 is tightly associated with lactate transporters MCT1 and MCT4 and facilitates their cell surface expression. EMBO J 19: 3896-3904.
136. De Saedeleer CJ, Porporato PE, Copetti T, Perez-Escuredo J, Payen VL, et al. (2014) Glucose deprivation increases monocarboxylate transporter 1 (MCT1) expression and MCT1-dependent tumor cell migration. Oncogene 33: 4060-4068.
137. Halestrap AP, Meredith D (2004) The SLC16 gene family-from monocarboxylate transporters (MCTs) to aromatic amino acid transporters and beyond. Pflugers Arch 447: 619-628.
138. Ullah MS, Davies AJ, Halestrap AP (2006) The plasma membrane lactate transporter MCT4, but not MCT1, is up-regulated by hypoxia through a HIF-1alpha-dependent mechanism. J Biol Chem 281: 9030-9037.
139. Bonuccelli G, Whitaker-Menezes D, Castello-Cros R, Pavlides S, Pestell RG, et al. (2010) The reverse Warburg effect: glycolysis inhibitors prevent the tumor promoting effects of caveolin-1 deficient cancer associated fibroblasts. Cell Cycle 9: 1960-1971.
140. Le Floch R, Chiche J, Marchiq I, Naiken T, Ilc K, et al. (2011) CD147 subunit of lactate/H+ symporters MCT1 and hypoxia-inducible MCT4 is critical for energetics and growth of glycolytic tumors. Proc Natl Acad Sci U S A 108: 16663-16668.
141. Rucci N, Recchia I, Angelucci A, Alamanou M, Del Fattore A, et al. (2006) Inhibition of protein kinase c-Src reduces the incidence of breast cancer metastases and increases survival in mice: implications for therapy. J Pharmacol Exp Ther 318: 161-172.
142. Avnet S, Salerno M, Zini N, Alberghini M, Gibellini D, et al. (2013) Sustained autocrine induction and impaired negative feedback of osteoclastogenesis in CD14(+) cells of giant cell tumor of bone. Am J Pathol 182: 1357-1366.
143. Ragni E, Vigano M, Rebulla P, Giordano R, Lazzari L (2013) What is beyond a qRT-PCR study on mesenchymal stem cell differentiation properties: how to choose the most reliable housekeeping genes. J Cell Mol Med 17: 168-180.
144. Livak KJ, Schmittgen TD (2001) Analysis of relative gene expression data using real-time quantitative PCR and the 2(-Delta Delta C(T)) Method.

Methods 25: 402-408.
145. Chomczynski P, Sacchi N (2006) The single-step method of RNA isolation by acid guanidinium thiocyanate-phenol-chloroform extraction: twenty-something years on. Nat Protoc 1: 581-585.
146. Andersen CL, Jensen JL, Orntoft TF (2004) Normalization of real-time quantitative reverse transcription-PCR data: a model-based variance estimation approach to identify genes suited for normalization, applied to bladder and colon cancer data sets. Cancer Res 64: 5245-5250.
147. Vandesompele J, De Preter K, Pattyn F, Poppe B, Van Roy N, et al. (2002) Accurate normalization of real-time quantitative RT-PCR data by geometric averaging of multiple internal control genes. Genome Biol 3: RESEARCH0034.
148. Hellemans J, Mortier G, De Paepe A, Speleman F, Vandesompele J (2007) qBase relative quantification framework and software for management and automated analysis of real-time quantitative PCR data. Genome Biol 8: R19.
149. Kase ET, Nikolic N, Bakke SS, Bogen KK, Aas V, et al. (2013) Remodeling of oxidative energy metabolism by galactose improves glucose handling and metabolic switching in human skeletal muscle cells. PLoS One 8: e59972.
150. Weinberg F, Hamanaka R, Wheaton WW, Weinberg S, Joseph J, et al. (2010) Mitochondrial metabolism and ROS generation are essential for Kras-mediated tumorigenicity. Proc Natl Acad Sci U S A 107: 8788-8793.
151. Oktem G, Bilir A, Uslu R, Inan SV, Demiray SB, et al. (2014) Expression profiling of stem cell signaling alters with spheroid formation in CD133/CD44 prostate cancer stem cells. Oncol Lett 7: 2103-2109.
152. Walker NJ (2002) Tech.Sight. A technique whose time has come. Science 296: 557-559.
153. Suvannasankha A, Chirgwin JM (2014) Role of bone-anabolic agents in the treatment of breast cancer bone metastases. Breast Cancer Res 16: 484.
154. Avnet S, Lamolinara A, Zini N, Solimando L, Quacquaruccio G, et al. (2006) Effects of antisense mediated inhibition of cathepsin K on human osteoclasts obtained from peripheral blood. J Orthop Res 24: 1699-1708.
155. Gilkerson RW, Selker JM, Capaldi RA (2003) The cristal membrane of mitochondria is the principal site of oxidative phosphorylation. FEBS Lett 546: 355-358.
156. Archer SL (2013) Mitochondrial dynamics--mitochondrial fission and fusion in human diseases. N Engl J Med 369: 2236-2251.
157. Rossignol R, Gilkerson R, Aggeler R, Yamagata K, Remington SJ, et al. (2004) Energy substrate modulates mitochondrial structure and oxidative capacity in cancer cells. Cancer Res 64: 985-993.

158. Williams JP, Blair HC, McDonald JM, McKenna MA, Jordan SE, et al. (1997) Regulation of osteoclastic bone resorption by glucose. Biochem Biophys Res Commun 235: 646-651.
159. Larsen KI, Falany ML, Ponomareva LV, Wang W, Williams JP (2002) Glucose-dependent regulation of osteoclast H(+)-ATPase expression: potential role of p38 MAP-kinase. J Cell Biochem 87: 75-84.
160. Su Y, Zhou A, Al-Lamki RS, Karet FE (2003) The a-subunit of the V-type H+-ATPase interacts with phosphofructokinase-1 in humans. J Biol Chem 278: 20013-20018.
161. Lu M, Holliday LS, Zhang L, Dunn WA, Jr., Gluck SL (2001) Interaction between aldolase and vacuolar H+-ATPase: evidence for direct coupling of glycolysis to the ATP-hydrolyzing proton pump. J Biol Chem 276: 30407-30413.
162. Mulari MT, Zhao H, Lakkakorpi PT, Vaananen HK (2003) Osteoclast ruffled border has distinct subdomains for secretion and degraded matrix uptake. Traffic 4: 113-125.
163. Zecchin A, Stapor PC, Goveia J, Carmeliet P (2015) Metabolic pathway compartmentalization: an underappreciated opportunity? Curr Opin Biotechnol 34: 73-81.
164. De Bock K, Georgiadou M, Schoors S, Kuchnio A, Wong BW, et al. (2013) Role of PFKFB3-driven glycolysis in vessel sprouting. Cell 154: 651-663.
165. Lee BS, Gluck SL, Holliday LS (1999) Interaction between vacuolar H(+)-ATPase and microfilaments during osteoclast activation. J Biol Chem 274: 29164-29171.
166. Salerno M, Avnet S, Alberghini M, Giunti A, Baldini N (2008) Histogenetic characterization of giant cell tumor of bone. Clin Orthop Relat Res 466: 2081-2091.
167. Nakajima EC, Van Houten B (2013) Metabolic symbiosis in cancer: refocusing the Warburg lens. Mol Carcinog 52: 329-337.
168. Sonveaux P, Copetti T, De Saedeleer CJ, Vegran F, Verrax J, et al. (2012) Targeting the lactate transporter MCT1 in endothelial cells inhibits lactate-induced HIF-1 activation and tumor angiogenesis. PLoS One 7: e33418.
169. Curtis KM, Gomez LA, Rios C, Garbayo E, Raval AP, et al. (2010) EF1alpha and RPL13a represent normalization genes suitable for RT-qPCR analysis of bone marrow derived mesenchymal stem cells. BMC Mol Biol 11: 61.
170. Siclari VA, Qin L (2010) Targeting the osteosarcoma cancer stem cell. J Orthop Surg Res 5: 78.
171. Monument MJ, Bernthal NM, Randall RL (2013) Salient features of mesenchymal stem cells-implications for Ewing sarcoma modeling. Front

Oncol 3: 24.
172. Kowalewska M, Danska-Bidzinska A, Bakula-Zalewska E, Bidzinski M (2012) Identification of suitable reference genes for gene expression measurement in uterine sarcoma and carcinosarcoma tumors. Clin Biochem 45: 368-371.
173. Rho HW, Lee BC, Choi ES, Choi IJ, Lee YS, et al. (2010) Identification of valid reference genes for gene expression studies of human stomach cancer by reverse transcription-qPCR. BMC Cancer 10: 240.
174. Thellin O, Zorzi W, Lakaye B, De Borman B, Coumans B, et al. (1999) Housekeeping genes as internal standards: use and limits. J Biotechnol 75: 291-295.
175. de Jonge HJ, Fehrmann RS, de Bont ES, Hofstra RM, Gerbens F, et al. (2007) Evidence based selection of housekeeping genes. PLoS One 2: e898.
176. Selvey S, Thompson EW, Matthaei K, Lea RA, Irving MG, et al. (2001) Beta-actin--an unsuitable internal control for RT-PCR. Mol Cell Probes 15: 307-311.

APPENDIX I

Publications arising from this work:

- Lemma S, Avnet S, Salerno M, Chano T, Baldini N. **Identification and validation of housekeeping genes for gene expression analysis of cancer stem cells.** *PLoS One. 2016 Feb 19;11(2):e0149481. doi:10.1371/journal.pone.0149481*

- Lemma S, Sboarina M, Porporato PE, Zini N, Sonveaux P, Di Pompo G, Baldini N, Avnet S**. Energy metabolism is finely tuned during osteoclast formation and function.** *Manuscript in preparation.*

The following papers were prepared during the doctoral training, although the material is not included in this thesis:

- Avnet S, Di Pompo G, Lemma S, Salerno M, Perut F, Bonuccelli G, Granchi D, Zini N, Baldini N. **V-ATPase is a candidate therapeutic target for Ewing sarcoma.** *Biochim Biophys Acta. 2013;1832:1105-16.*
- Evangelisti C, Bernasconi P, Cavalcante P, Cappelletti C, D'Apice MR, Sbraccia P, Novelli G, Prencipe S, Lemma S, Baldini N, Avnet S, Squarzoni S, Martelli AM, Lattanzi G. **Modulation of TGFbeta 2 levels by lamin A in U2-OS osteoblast-like cells: understanding the osteolytic process triggered by altered lamins.** *Oncotarget. 2015;6:7424-37.*
- Avnet S, Lemma S, Cortini M, Pellegrini P, Perut F, Cesari V, Zini N, Kusuzaki K, Chano T, Grisendi G, Dominici M, De Milito A, Baldini N. **The altered pH gradient at the plasma membrane is a crucial mechanism of chemoresistance of human osteosarcoma.** *Manuscript in preparation.*